SISSA
Scuola
Internazionale
Superiore di
Studi Avanzati

Neuroscience Area – PhD course in Molecular Biology

AGGREGATION STUDIES ON THE TRANSACTIVE RESPONSE DNA BINDING PROTEIN OF 43 KDA (TDP-43)

Candidate:
Carlo Scialò

Advisor:
Prof. Giuseppe Legname

Academic Year 2019-20

Supervisor:	**Prof. Giuseppe Legname, Ph.D.**
External examiners:	**Prof. Emanuele Buratti, Ph.D.**
	Prof. Gianluigi Zanusso, Ph.D.

TABLE OF CONTENTS:

ABSTRACT 1

LIST OF ABBREVIATIONS: 3

CHAPTER I 6

1. INTRODUCTION 6
1.1 Neurodegenerative disorders as conformational diseases 6
1.2 TDP-43 Proteinopathies 7
1.2.1 Clinical, genetic and histopathological heterogeneity of ALS and FTLD 7
1.2.2 Histopathological classification of TDP-43 proteinopathies 11
1.3 TDP-43 structure and functions 14
1.3.1 TDP-43 structure 14
1.3.2 TDP-43 functions 17
1.4 The prion-like hypothesis for neurodegenerative diseases 20
1.4.1 TDP-43 prion-like properties 22
1.4.2 TDP-43 strains 25
1.5 TDP-43 as a disease biomarker 27
1.6 The real time quaking induced conversion reaction 29

CHAPTER II 32

2. AIMS OF THE STUDY 32

CHAPTER III 33

3. MATERIALS AND METHODS 33
3.1 Recombinant full-length and truncated TDP-43 production 33
3.2 Electrophoretic Mobility Shift Assay (EMSA) 34
3.3 Brain homogenates (BH) collection e preparation 34
3.4 CSF samples collection and study population 35
3.5 *In vitro* generation of recombinant human TDP-43 aggregates 36
3.6 TDP-43 RT-QuIC optimization 37
3.7 CSF TDP-43 seeds detection with RT-QuIC 38
3.8 Immune-depletion of TDP-43 species 39

3.9 *In vitro* generation of recombinant human α-synuclein and tau K18 aggregates 40
3.10 Atomic force microscopy analysis 40
3.11 Lag phase threshold definition 40
3.12 Statistical analysis 41
3.13 Cell culture and transfection 42
3.14 Treatment with HuTDP-43(263-414) fibrils 42
3.14.1 Fluorescence imaging 42
3.15 Cell vitality assay (MTT) 43
3.16 Standard RT-PCR and RT-qPCR analysis 43

CHAPTER IV 45

4. RESULTS 45
4.1 Part I-development and optimization of the TDP-43 RT-QuIC 45
4.1.1 Recombinant full-length and truncated TDP-43 production 45
4.1.2 Adaptation of RT-QuIC to TDP-43 amplification 47
4.1.3 TDP-43 RT-QuIC optimization 48
4.1.4 CSF TDP-43 seeds detection with RT-QuIC 51
4.1.5 Performance of TDP-43 RT-QuIC with tau and α-synuclein aggregates 58
4.1.6 RT-QuIC detection of aggregated TDP-43 59
4.2 Part II-uptake and toxicity of synthetic TDP-43 aggregates 60
4.2.1 TDP-43 fibrils uptake and phosphorylation in SH-SY5Y cells 60
4.2.2 TDP-43 fibrils recruit endogenous TDP-43 to form intra-cellular aggregates 61
4.2.3 TDP-43 aggregates are toxic to cells and maintain RNA-binding ability 62

CHAPTER V 66

5. DISCUSSION 66
5.1 Development and optimization of the TDP-43 RT-QuIC 66
5.2 Uptake and toxicity of synthetic TDP-43 aggregates 68
5.3 Conclusions 70

APPENDIX 72

SUPPLEMENTARY MATERIALS 72

REFERENCES 74

ABSTRACT

The pathological deposition of the transactive response DNA-binding protein of 43 kDa (TDP-43) occurs in the majority (~97%) of amyotrophic lateral sclerosis (ALS) and in around 45% of frontotemporal lobar degeneration cases (FTLD). ALS and FTLD clinically overlap, presenting a continuum of phenotypes. Both ALS and FTLD lack treatments able to interfere with the underlying pathological process and early detection of TDP-43 pathology would facilitate the development of disease modifying drugs. The Real Time Quaking Induced Conversion reaction (RT-QuIC) showed the ability to detect prions in several peripheral tissues of patients with different forms of prion and prion-like diseases. Despite TDP-43 displays prion-like properties, to date the RT-QuIC technology has not yet been adapted to this protein. The main aim of this study was to adapt the RT-QuIC technique for the TDP-43 substrate and to exploit the intrinsic ability of this technology to amplify minutes amount of misfolded proteins for the detection of pathological TDP-43 species in the CSF of ALS and FTLD patients. As a second objective, we aimed at performing a preliminary evaluation of the seeding properties of the *in vitro* obtained TDP-43 synthetic aggregates, in order to evaluate their ability to recapitulate ALS/FTD TDP-43 pathology. First, we adapted the RT-QuIC technique for the aggregation of the TDP-43 substrate and then we optimized it with synthetic TDP-43 preformed aggregates and with autopsy-verified brain homogenate samples. After this optimization, we analyzed CSF samples from ALS and FTLD patients and controls. TDP-43 RT-QuIC was able to detect as little as 15 picograms of TDP-43 aggregates, discriminating between a cohort of subjects affected by ALS and FTLD and age-matched controls, with a total sensitivity of 94% and a specificity of 85%. Our preliminary analysis of HuTDP-43(263-414) fibrils showed that they were readily internalized and actively phosphorylated in SH-SY5Y cells. Furthermore, they were able to recruit the full-length endogenous protein in the formation of intra-cellular

aggregates composed of hyperphosphorylated forms of the protein. We observed that the formation of TDP-43 intra-cellular aggregates resulted in a severe reduction of cell vitality which was not linked to a TDP-43 loss of function, but potentially related to a maintained RNA-binding capacity of TDP-43 aggregates. In conclusion, our data represent a proof-of-concept of TDP-43 RT-QuIC potential for the detection of TDP-43 pathological aggregates. Together with prion, amyloid beta, tau and α-syn RT-QuIC assays, a further optimization of the presented TDP-43 RT-QuIC protocol, would increase the opportunity to perform the earliest and most accurate diagnosis at a single patient level. Furthermore, we show that CSF detection of TDP-43 pathological aggregates may be exploited as a disease biomarker for ALS and FTLD. Our preliminary results regarding the seeding properties of TDP-43 synthetic aggregates suggest that TDP-43 RT-QuIC could be exploited not only as a powerful drug screening and diagnostic tool but could also serve as a very helpful instrument to further elucidate TDP-43 prion-like features.

LIST OF ABBREVIATIONS:

α-syn:	α-synuclein
AD:	Alzheimer's disease
AFM:	atomic force microscopy
ALS:	amyotrophic lateral sclerosis
ALSbi:	ALS behavioral impairment
ALSci:	ALS cognitive impairment
avPPA:	agrammatic variant of primary progressive aphasia
Aβ:	amyloid-beta
BH:	brain homogenate
BSA:	bovine serum albumin
bv-FTD:	behavioral variant of frontotemporal dementia
CBD:	cortico-basal degeneration
CBS:	cortico-basal syndrome
CNS:	central nervous system
CTFs:	C-terminal fragments
ddH2O:	bi-distilled water
DNs:	dystrophic neurites
DTT:	dithiothreitol
EDTA:	ethylenediaminetetraacetic acid
EMSA:	electrophoretic mobility shift assay
FBS:	fetal bovine serum
FPR:	false positive rate
FTD:	frontotemporal dementia
FTLD:	frontotemporal lobar degeneration

GdnHCl: guanidine hydrochloride

GFNIs: granulo-filamentous neuronal inclusions

G-PDC: dementia parkinsonism ALS complex of Guam

HD: Huntington's disease

hnRNPs: heterogeneous ribonucleoproteins

IPTG: β-D-1 thiogalactopyranoside

LARKS: low-complexity aromatic-rich kinked segments

LBD: Lewy body disease

LCD: low-complexity domain

LLPS: liquid-liquid phase separation

LP: lumbar puncture

MCI: mild cognitive impairment

MND: motor neuron disease

MSA: multiple system atrophy

MTT: 3-(4,5-dimethylthiazol- 2-yl)-2,5-diphenyltetrazolium bromide

naPPA: progressive non-fluent/agrammatic aphasia

NCI: neuronal cytoplasmic inclusions

NES: nuclear export signal

NGS: normal goat serum

NIIs: neuronal intranuclear inclusions

NLS: nuclear localization signal

NTD: N-terminal domain

PD: Parkinson's disease

PK: proteinase K

PrP: prion protein

PrP^{C}: physiological cellular form of PrP

PrP^{Sc}:	misfolded, pathogenic form of PrP, or PrP scrapie
PSP:	progressive supranuclear palsy
RFU:	relative fluorescence unit
ROC:	receiver operating characteristic
RRM:	RNA recognition motif
RT:	room temperature
RT-qPCR:	real time quantitative polymerase chain reaction
RT-QuIC:	real time quaking induced conversion reaction
SDS:	sodium dodecyl sulfate
SG:	stress granule
svPPA:	semantic dementia
TDP-43:	transactive response DNA-binding protein of 43 kDa
ThT:	thioflavin T
TPR:	true positive rate
TSE:	transmissible spongiform encephalopathies

CHAPTER I

1. INTRODUCTION

1.1 Neurodegenerative disorders as conformational diseases

Neurodegenerative diseases (NDDs) are characterized by progressive dysfunction and loss of neurons leading to the involvement of specific functional systems defining, ultimately, their clinical presentations. NDDs include transmissible spongiform encephalopathies (TSEs), Alzheimer's disease (AD), Parkinson's disease (PD), multiple system atrophy (MSA), amyotrophic lateral sclerosis (ALS), frontotemporal lobar degeneration (FTLD), Huntington's disease (HD), progressive supranuclear palsy (PSP), cortico-basal degeneration (CBD) and many others.

Although their differences in terms of clinical and neuropathological features, increasing evidence suggests that these disorders share a common pathogenic feature: the presence in the Central Nervous System (CNS) of deposits of misfolded proteins with altered physicochemical properties (Kovacs, 2016). Consequently, NDDs can be classified according to the predominant deposited protein in the brain, leading to the definition of proteinopathies or conformational diseases (Maniecka and Polymenidou, 2015). Placing proteins in the center of the pathogenesis of NDDs led to several implications, among which the development of novel approaches to identify disease biomarkers and to develop innovative therapeutic strategies.

The main protein component of pathological deposits may be unique for each disorder, e.g. α-synuclein in PD, while in other conditions more than one misfolded protein can be involved, as for instance in AD where there is the co-presence of tau-positive neurofibrillary tangles together with amyloid-β (Aβ) plaques. Misfolded pathological proteins can accumulate in the intra- or

the extra-cellular space (Kovacs, 2016). Extracellular deposits comprise aggregates with immunoreactivity for Aβ or the prion protein (PrP), while proteins found in intracellular deposits include tau, α-synuclein and TAR DNA-binding protein 43 (TDP-43).

1.2 TDP-43 Proteinopathies

The interest for the nuclear RNA binding protein (RBP) TDP-43 as a key player in neurodegeneration started in 2006, when it was first reported as the main protein component of aggregates in neurons of patients affected by ALS and FTLD (Arai *et al.*, 2006; Neumann *et al.*, 2006). Following these first reports, the abnormal accumulation of TDP-43 has been increasingly observed in neurodegenerative disorders other than FTLD and ALS, as for instance dementia with Lewy bodies (Nakashima-Yasuda *et al.*, 2007; Lin and Dickson, 2008; Arai *et al.*, 2009), CBD (Uryu *et al.*, 2008), PSP (Yokota *et al.*, 2010), dementia parkinsonism ALS complex of Guam (G-PDC) (Hasegawa *et al.*, 2007), Pick's disease (Freeman *et al.*, 2008; Lin and Dickson, 2008), hippocampal sclerosis (Amador-Ortiz *et al.*, 2007; Yokota *et al.*, 2010), AD, HD and PD (Nakashima-Yasuda *et al.*, 2007; Arai *et al.*, 2009; Josephs *et al.*, 2016). Neurodegenerative disorders linked to the primary deposition of TDP-43, as ALS and FTLD, are collectively named TDP-43 proteinopathies (Nonaka and Hasegawa, 2018).

1.2.1 Clinical, genetic and histopathological heterogeneity of ALS and FTLD

ALS is clinically characterized by an adult onset focal muscle weakness and wasting, that most commonly starts in the limb muscles (more frequently in distal than in proximal muscles) and tends to spread and progress relentlessly. In around 30% of cases the disease presents a bulbar onset, characterized by dysarthria, dysphonia and dysphagia. There is a high degree of

variability in the age at onset, the site of onset and the disease progression rate of ALS. The disease commonly presents the fatal and progressive involvement of an increasing number of muscular districts and in the majority of cases has a median survival of 3 years from symptom onset, with the *exitus* mainly due to respiratory failure (Masrori and Van Damme, 2020). It is now well recognized that ALS can exist as a pure motor syndrome but that it can coexist with a frontotemporal dementia (Strong *et al.*, 2009) (ALS-FTD) as defined by the Neary or Hodges criteria (Neary *et al.*, 1998; Hodges and Miller, 2001). Behavior and/or cognitive features, not sufficient to meet criteria for the diagnosis of dementia but enough to be detected, could also be present (termed ALS behavioral impairment, ALSbi, and ALS cognitive impairment, ALSci, respectively). Furthermore, a small population of ALS patients could develop dementia not typical of FTD (ALS-Dementia) (Strong *et al.*, 2009).

Frontotemporal dementia (FTD) is a clinically and pathologically heterogeneous group of non-Alzheimer dementias characterized collectively by the degeneration of frontal and anterior temporal lobes (FTLD) and clinically defined by behavioral changes, alterations of executive functioning and/or language impairment (Neary *et al.*, 1998). Patients may present a broad spectrum of clinical signs and symptoms ranging from behavioral/executive alterations with or without motor neuron dysfunction to language impairment (Irwin *et al.*, 2015). There are three main clinical syndromes of FTD, defined on the basis of leading features at presentation. About half of cases present with behavioral change (behavioral variant frontotemporal dementia, bvFTD), and the remainder present with language decline (primary progressive aphasia, PPA) characterized either by impaired speech production (progressive non-fluent/agrammatic aphasia, naPPA) or by impaired word comprehension and semantic memory (semantic dementia, svPPA) (Gorno-Tempini *et al.*, 2011; Rascovsky *et al.*, 2011; Warren *et al.*, 2013).

ALS and FTD are now considered to be linked clinically, pathologically and mechanistically and to represent a continuum of a broad neurodegenerative disorder, presenting in a spectrum

of overlapping clinical symptoms, with ALS patients displaying cognitive impairment or signs of FTD in approximately 50% and 15% of the cases, respectively (Ling *et al.*, 2013) (Figure 1). ALS can present in sporadic (90% of cases) or familial (10%) forms, the latter characterized by the presence of more than one case in the same family. Familial (fALS) and sporadic ALS (sALS) cases are clinically indistinguishable. The five most common genetic causes of ALS are the hexanucleotide expansion in chromosome 9 open reading frame 72 (*C9orf72*) and mutations in superoxide dismutase 1 (*SOD1*), TAR DNA-binding protein 43 (*TARDBP*), fused in sarcoma/translated in liposarcoma (*FUS/TLS*) and TANK-binding kinase 1 (*TBK1*).

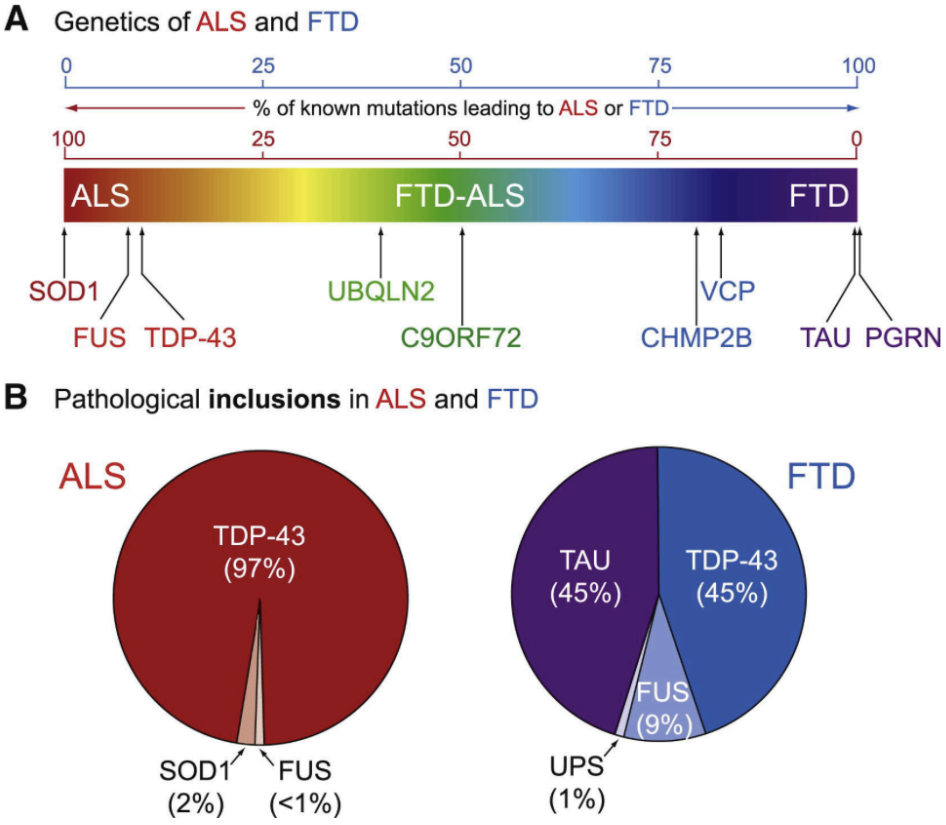

Figure 1: Clinical, Genetic, and Pathological Overlap of ALS and FTD. (**A**) ALS and FTD represent a continuum of a broad neurodegenerative disorder, presenting in a spectrum of overlapping clinical symptoms (ALS in red and FTD in purple). Major known genetic causes for ALS and FTD are plotted according to the ratio of known mutations that give rise to ALS

or FTD. (**B**) Pathological protein inclusions in ALS and FTD, according to the major protein accumulated. From: (Ling *et al.*, 2013).

Together, they explain about 15% of all ALS patients and over 50% of the familial cases (Ling *et al.*, 2013; Masrori and Van Damme, 2020).

FTD presents a stronger genetic contribution than ALS, suggested by the higher percentage of familial cases (around 50%). The first two identified causal genes for FTD are the one for the microtubule-associated protein tau (*MAPT*) (Hutton *et al.*, 1998) and for progranulin (*GRN*) (Baker *et al.*, 2006; Cruts *et al.*, 2006), which together account for 10%–20% of FTD (Van Langenhove *et al.*, 2012). More rarely, mutations in *TARDBP* and *FUS/TLS* are causal for FTD (Lagier-Tourenne *et al.*, 2010). The hexanucleotide expansion in the *C9ORF72* gene was found to be a common genetic cause for ALS and FTD, accounting for approximately one-third of cases of familial FTD and fALS cases and for 4% to 21% of patients with apparently sporadic disease (DeJesus-Hernandez *et al.*, 2011; Renton *et al.*, 2011).

ALS-, ALS/dementia-, and/or FTD-causing mutations were also identified in genes involved in protein clearance pathways or maintaining adequate protein homeostasis, including ubiquilin-2 (*UBQLN2*) (Deng *et al.*, 2011), valosin-containing protein (*VCP*) (Johnson *et al.*, 2010), vesicle-associated membrane protein-associated protein B (*VAPB*) (Nishimura *et al.*, 2004), p62/sequestosome (*SQSTM1*) (Teyssou *et al.*, 2013), optineurin (*OPTN*) (Maruyama *et al.*, 2010), and charged multivesicular body protein 2B or chromatin modifying protein 2B (*CHMP2B*) (Parkinson *et al.*, 2006), with the list continuously enlarging because of newly identified players.

This extremely complex genetic background is partially reflected in the diversity of the pathological inclusions observed in ALS and FTD affected subjects. As depicted in Figure 1 the majority of ALS cases present the deposition of the TDP-43 protein, with the exception of the ones linked to *SOD-1* or *FUS/TLS* mutations, while for FTD the scenario is more complex.

This includes four main groups: FTLD-tau (45%), FTLD-TDP (45%), FTLD-FUS (9%), and a remaining 1% named FTLD-UPS (ubiquitin-proteasome system) (Figure 1). Mutations in the *GRN* and *TARDBP* gene and the presence of the *C9orf72* expansion are all invariantly associated with TDP-43 pathology in the CNS (Sieben *et al.*, 2012). These findings highlight the central role of TDP-43 as the major protein component of pathological inclusions observed in over 90% of ALS and around 50% of FTD patients.

1.2.2 Histopathological classification of TDP-43 proteinopathies

Biochemical and immunohistochemical studies showed that TDP-43 accumulated in ALS/FTLD pathological aggregates displays characteristic features of intracellular amyloid-like proteins, similar to those observed in other neurodegenerative disorders, as tauopathies or synucleinopathies. More in details, within the insoluble TDP-43-positive pathological aggregates, the protein is hyperphosphorylated, ubiquitinated (also p62-positive) and abnormally cleaved to generate C-terminal fragments (CTFs) (Nonaka and Hasegawa, 2018). Furthermore, neuronal cytoplasmic TDP-43 aggregates are associated with loss of physiological nuclear TDP-43 (Neumann *et al.*, 2006). According to the shape and distribution of TDP-43 positive lesions within the CNS, several studies identified distinct histopathological patterns of TDP-43 pathology in FTLD-TDP leading to a harmonized classification in four subtypes (from A to D) (Mackenzie *et al.*, 2011), recently extended due to the description of a further one, type E (Lee *et al.*, 2017). Interestingly, there is a relatively strong association between each histopathologic subtype and various clinical and/or genetic features of the disease (Mackenzie *et al.*, 2006; Geser *et al.*, 2009; Josephs *et al.*, 2009; Mackenzie *et al.*, 2011). Type A cases are associated with behavioral variant of frontotemporal dementia (bvFTD) or nonfluent/agrammatic primary progressive afasia (naPPA), together with disease-causing

mutations in the progranulin gene, *GRN*. Type B cases are associated with bvFTD including cases with motor neuron disease (MND), together with disease-causing expansions in *C9orf72*. Type C cases are associated with bvFTD or semantic variant PPA (svPPA) and are typically sporadic FTD having no association with any known disease-causing genetic mutations. Type D histopathology is associated with mutations in valosin-containing protein (VCP) that cause familial inclusion body myositis, Paget's disease of bone, FTD, and/or ALS, variably called either IBMPFD-ALS or multisystem proteinopathy. Finally, the recently described type E cases present no clear association with any specific genetic background and are mainly associated with bvFTD with a rapidly progressive clinical course (Neumann *et al.*, 2007b; Lee *et al.*, 2017). Ubiquitin- and TDP-43-positive pathological inclusions include neuronal cytoplasmic inclusions (NCIs), dystrophic neurites (DNs), neuronal intranuclear inclusions (NIIs), glial cytoplasmic inclusions and granulo-filamentous neuronal inclusions (GFNIs). Type A is characterized by crescentic to oval ring-like NCIs and many short DNs involving superficial neocortical layers. Lentiform NIIs and oligodendroglial inclusions may also be observed. Type B is characterized by NCIs affecting superficial and deep cortical layers with a paucity of DNs. Rare oligodendroglial inclusions may be observed. Type C is characterized by long DNs predominantly in superficial layers with a paucity of NCIs. Type D is characterized by frequent lentiform NIIs with short DNs. Finally, Type E is characterized by abundance of granulo-filamentous neuronal inclusions and very fine, dot-like neuropil aggregates affecting all neocortical layers in addition to curvilinear oligodendroglial inclusions in the white matter (Lee *et al.*, 2017). Figure 2 recapitulates the main features of TDP-43 histopathological classification.

The sarkosyl-insoluble fraction extracted from ALS and FTLD-TDP cases immunoblotted with an anti-TDP-43 antibody, which recognizes only the aberrantly phosphorylated fraction of the protein, presents a specific banding pattern. This is characterized by the presence of the

hyperphosphorylated full-length TDP-43 at ~45 kDa, smearing substances and CTFs at 18–26 kDa, which are not observed in control samples (Hasegawa *et al.*, 2008; Inukai *et al.*, 2008; Nonaka and Hasegawa, 2018). Interestingly enough, immunoblot analysis also reveals a correspondence between the banding patterns of CTFs of insoluble TDP-43 and the neuropathological subtype, suggesting that TDP-proteinopathies can be classified not only based on histological features but also biochemically (Nonaka and Hasegawa, 2018).

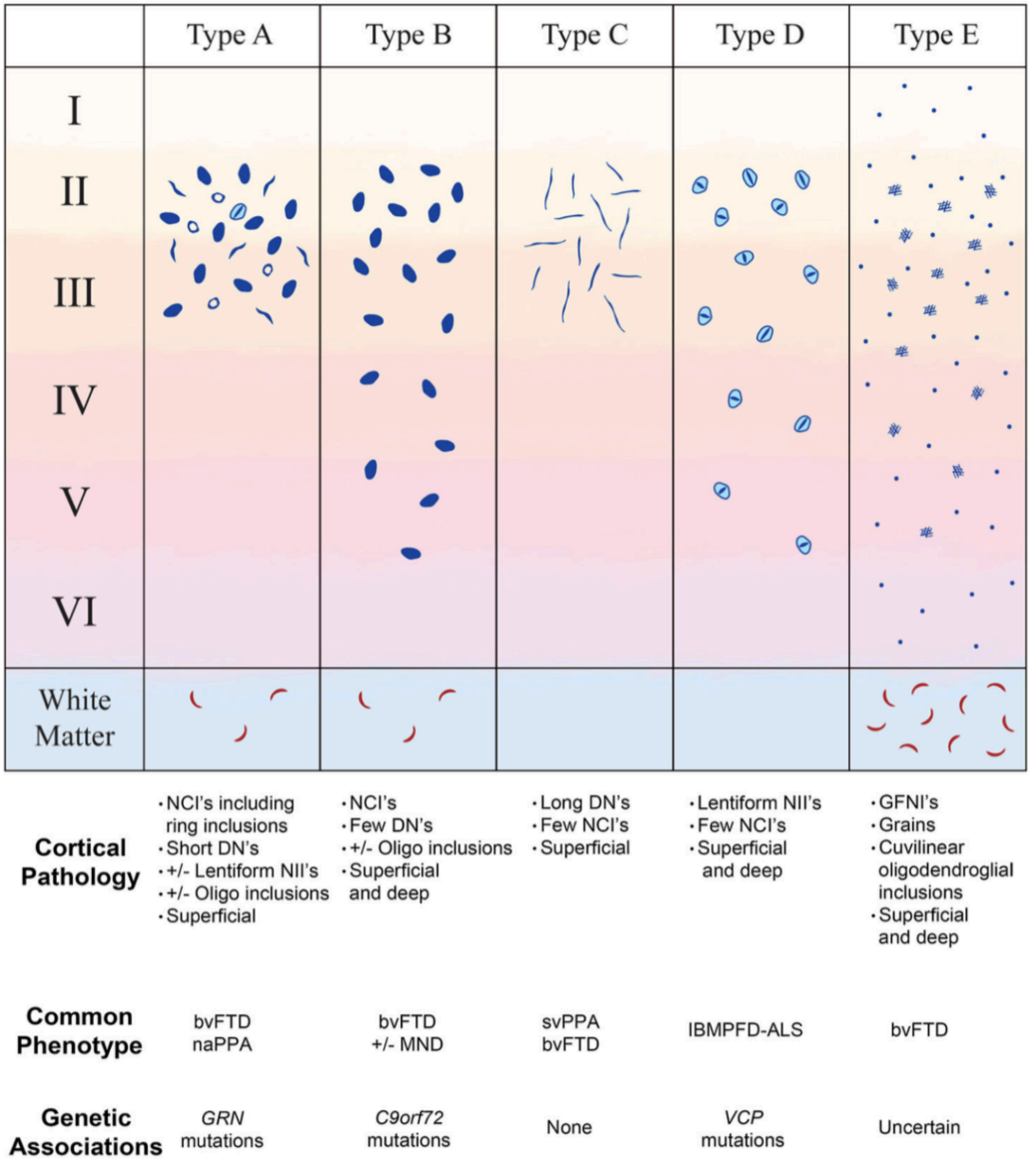

Figure 2: Main features of TDP-43 histopathological classification. NCIs: neuronal cytoplasmic inclusions; DNs: dystrophic neurites; NIIs: neuronal intranuclear inclusions; GFNIs: granulo-filamentous neuronal inclusions; bvFTD: behavioral variant of frontotemporal

dementia; naPPA: nonfluent/agrammatic primary progressive afasia (PPA); svPPA: semantic variant PPA; MND: motor neuron disease; IBMPFD: familial inclusion body myositis Paget's disease of bone; ALS: amyotrophic lateral sclerosis. From: (Lee *et al.*, 2017).

Furthermore, each specific banding pattern of the extracted insoluble TDP-43 CTFs could be related to different cleavage sites of the pathological protein, suggesting the presence of multiple insoluble TDP-43 conformers, a feature reminiscent of prion strains (Nonaka and Hasegawa, 2018; Scialo *et al.*, 2019). This concept has been recently supported by a study from Laferriere et al., which exploited a new method to isolate insoluble TDP-43 pathological aggregates from diseased brain and showed that each histopathological subtype displays specific morphology, biochemical features and seeding properties (Laferriere *et al.*, 2019) (this study will be discussed in more details in section 1.4).

1.3 TDP-43 structure and functions

1.3.1 TDP-43 structure

TDP-43 is a 414 amino acids (aa) long protein encoded by the TARDBP gene, located at chromosome 1 and composed of six exons (Francois-Moutal *et al.*, 2019). TDP-43 belongs to the family of the heterogeneous ribonucleoproteins (hnRNPs), sharing with them several structural and functional features (Afroz *et al.*, 2019). TDP-43 possesses all the domains of a classical hnRNP protein: N-terminal and C-terminal regions used for protein-protein interactions and two RNA recognition motifs (RRMs) to bind target RNA, mostly in a sequence-specific manner (Ratti and Buratti, 2016). TDP-43 is composed of a modular multi-domain architecture encompassing an N-terminal domain (NTD), two RRMs and a glycine-rich, intrinsically disordered C-terminal low complexity region (LCD). Additionally, TDP-43

presents a bipartite nuclear localization signal (NLS) and a predicted nuclear export signal (NES) (Figure 3) (Ling *et al.*, 2013; Afroz *et al.*, 2019).

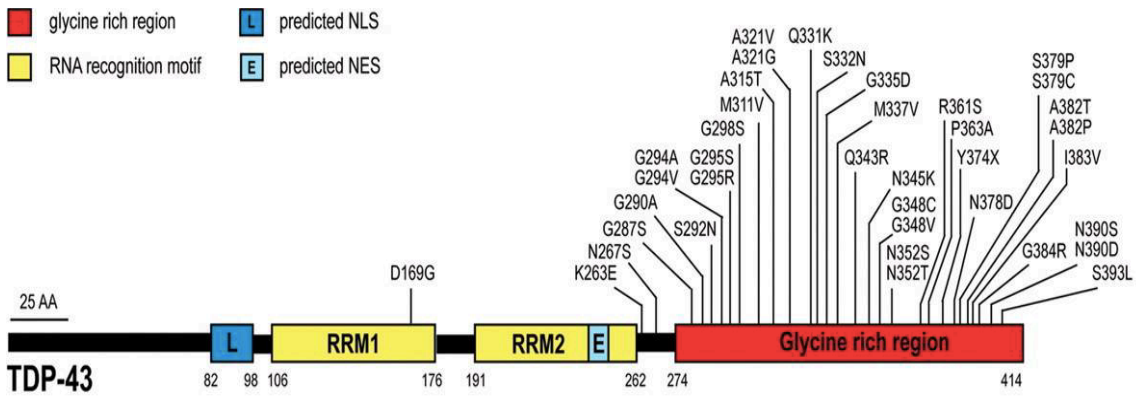

Figure 3: TDP-43 structure and its pathological mutations. TDP-43 is a 414 aa protein encoded by six exons and containing a structured N-terminal domain, two RNA recognition motifs (RRM1 and RRM2) and a C-terminal glycine-rich region. Most of the pathological mutations identified are localized in the glycine-rich region encoded by exon 6. Modified from: (Lagier-Tourenne *et al.*, 2010).

TDP-43 is localized preferentially in the nucleus and the NLS sequence allows the protein to continuously shuttle between this compartment and the cytoplasm. The NLS is located in the linker region between the NTD and the RRMs while the two putative NES sequences are located within the RRM2. Recently, it has been shown that neither of the two NES are functional and that TDP-43 exits the nucleus by passive diffusion, as other RNA-binding proteins, like FUS/TLS (Ederle *et al.*, 2018). The folded NTD (aa 1-80) is structurally composed of six β-strands and a single α-helix, arranged in a ubiquitin-like β-grasp fold, similar to the DIX domain of Axin 1 (Mompean *et al.*, 2016). It has been suggested that the NTD is involved in the oligomerization of nuclear TDP-43 molecules through a head-to-tail interaction, facilitating TDP-43 molecules oligomerization in association with nucleic acids (a critical step

for splicing regulation) and impeding detrimental interactions among the LCDs, thus preventing the pathological aggregation of the protein (Afroz *et al.*, 2017). The two RRMs of the protein span amino acids 106–177 (RRM1) and 192–259 (RRM2) and contain two highly conserved short sequence motifs known as RNP-1 (octameric sequence: KGFGFVRF in RRM1 and RAFAFVTF in RRM2) and RNP-2 (hexameric sequence: LIVLGL in RRM1 and VFVGRC in RRM2) (Francois-Moutal *et al.*, 2019). Thanks to its RRMs, TDP-43 can bind to both DNA and RNA molecules in a sequence-specific manner with preference towards TG/UG-rich sequences (Ishiguro *et al.*, 2016). The RRMs are able to bind 3-4 UG repeat *per* TDP-43 molecule, and structural analysis of tandem RRMs in complex with UG-rich RNA suggested a unique mode of RNA binding for TDP-43, characterized by the formation of a continuous RNA binding surface, allowing the binding of longer RNA sequences (Lukavsky *et al.*, 2013; Afroz *et al.*, 2019). The C-terminal region of TDP-43 (aa 261-414) is a low complexity glycine-rich region that, isolated in solution, is primarily unstructured, but contains a short α-helix (aa 311-347) (Afroz *et al.*, 2019). TDP-43 LCD is the site of about 50 disease-linked mutations (Mackenzie and Rademakers, 2008) (Figure 3) as well as most of the phosphorylation sites. Due to its intrinsically disordered nature, all structural studies of this region have been of fragments. Distinct subdomains of the LCD have been described: two Gly-aromatic-Ser-rich (GaroS) regions, an amyloidogenic core divided into a hydrophobic region and a Q/N-rich region (Mompean *et al.*, 2016). The GaroS regions (residues 273–317 and 368–414) are similar to FUS/TLS domains (Murray *et al.*, 2017) proposed to interact within RNA granules (Mompean *et al.*, 2016) and contributing to the formation of hydrogels (Kato *et al.*, 2012). The hydrophobic region (residues 318–340) can adopt either a helical structure or Thioflavin T-positive filament cross-β architecture (Jiang *et al.*, 2013). Furthermore, multiple short segments of TDP-43 LCD have been shown to form either steric zippers or reversible (velcro-like) beta-sheet enriched structures called low-complexity aromatic-rich kinked segments (LARKS),

thought to play a role in complex protein interactions and in TDP-43 pathological aggregation (Guenther *et al.*, 2018). TDP-43 LCD likely adopts a range of transient well-ordered shapes, many of which are capable of self-association. Mutations and post-translational modifications may change the kinetics of these states, influencing the balance between fibril formation and dissolution (Francois-Moutal *et al.*, 2019). The TDP-43 LCD has multiple functions and has been shown to mediate protein-protein interaction, to participate in the stabilization of protein-RNA interactions and to be required for TDP-43 splicing activity (Buratti *et al.*, 2001; Ayala *et al.*, 2005; Buratti *et al.*, 2005; Afroz *et al.*, 2019), including autoregulation (Ayala *et al.*, 2011). Finally, TDP-43 C-terminal domain can phase separate into liquid droplets, a process generally called LLPS (liquid-liquid phase separation) which is thought to be a facilitating event leading to the formation of membrane-less organelles, as stress granules (SGs), and to potentially allow an increase in protein concentration at specific locations inside the cell (Dewey *et al.*, 2011; Han *et al.*, 2012; Molliex *et al.*, 2015; Conicella *et al.*, 2016; Gasset-Rosa *et al.*, 2019; Mann *et al.*, 2019). Both these events could potentially favor TDP-43 pathological aggregation *via* the interaction of the LCDs of several TDP-43 molecules or of LCDs of multiple RNA-binding proteins within SGs, although LLPS was recently described to be independent from SGs formation (Gasset-Rosa *et al.*, 2019; Mann *et al.*, 2019).

1.3.2 TDP-43 functions

TDP-43 was first identified as a protein factor capable of repressing the transcription of human immunodeficiency virus type 1 (HIV-1) *via* binding to its regulatory transactivation response element (TAR) (Ou *et al.*, 1995). Despite TDP-43 was later shown to be ineffective in modifying HIV-1 replication in human cells (Nehls *et al.*, 2014), the protein maintained this named derived from that first description (TAR DNA-binding protein of 43 kDa). The role of

TDP-43 in transcription control was subsequently confirmed by the observation of its association with transcriptionally-enriched euchromatin in rat neurons and human brain (Thorpe *et al.*, 2008; Casafont *et al.*, 2009). TDP-43 plays multiple and relevant roles related to RNA processing, including the regulation of alternative splicing, RNA maturation, stability and transport (Afroz *et al.*, 2019).

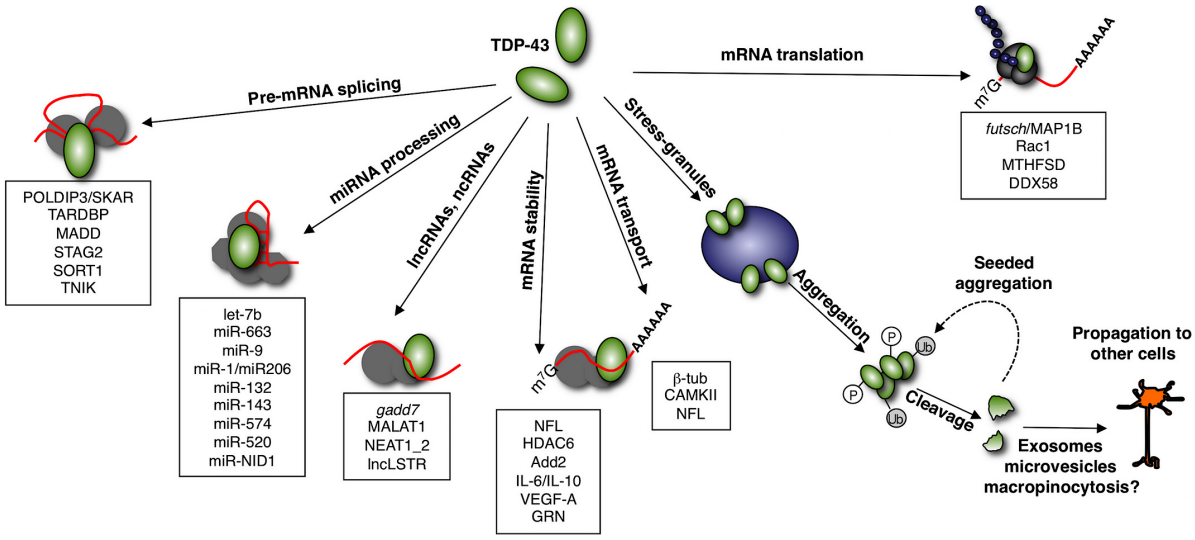

Figure 4: TDP-43 functions. Schematic representation of TDP-43 functions in the nuclear and cytoplasmic compartments. Each box reports the names of validated TDP-43 RNA targets. From: (Ratti and Buratti, 2016).

The first described RNA target of TDP-43 regulatory function on alternative splicing is the cystic fibrosis transmembrane conductance regulator (CFTR), whose regulation is mediated in cooperation with other hnRNPs, like the SR proteins (Buratti *et al.*, 2001). The strongest confirmation of the central role played by TDP-43 in RNA metabolism regulation emerged ten years later with the genome-wide identification of several hundreds of RNA targets in human and mouse brain (Polymenidou *et al.*, 2011; Tollervey *et al.*, 2011). TDP-43 binds to many nascent RNA molecules, both pre-mRNA and non-coding RNAs, playing a crucial role in

regulating their destiny and functionality (Polymenidou *et al.*, 2012). It preferentially binds to long intronic regions of neuronal gene transcripts and this binding is crucial to sustain their physiological levels (Polymenidou *et al.*, 2011). The second most enriched TDP-43 binding sites are located near intron-exon junctions, leading to the modulation of the alternative splicing of the flanking exons. This function is mediated by the cooperation with other hnRNPs and can lead to either the inclusion or exclusion of the flanking exon depending on the location of the binding site (Polymenidou *et al.*, 2011).

TDP-43 participates in in the formation of Drosha and Dicer complexes, thus regulating the biogenesis and expression of several miRNAs (Kawahara and Mieda-Sato, 2012). TDP-43 is primarily located to the nucleus, nevertheless thanks to its NLS it actively shuttles between this compartment and the cytoplasm, where it binds the 3'-UTR of its mature mRNA targets (Tollervey *et al.*, 2011). Importantly, one of TDP-43 targets is the 3'-UTR of its own mRNA which it binds to finely regulate its stability and translation (Polymenidou *et al.*, 2011). Two different modes of TDP-43 self-regulation have been described which can act in combination to regulate TDP-43 cellular levels (Avendano-Vazquez *et al.*, 2012; D'Alton *et al.*, 2015). For other mRNA targets, TDP-43 controls either their stability, transport or translation, this last mechanism mediated by its interaction with proteins involved in translation initiation and elongation factors (Freibaum *et al.*, 2010). TDP-43 may also be implicated in the transport of specific mRNAs to distal cellular sites, suggesting a role in the control of spatial translation in specific compartments, as for instance axons terminals and synapsis (Alami *et al.*, 2014). Finally, as already described in the previous section, the ability of TDP-43 to phase separate into liquid droplets facilitates its recruitment into stress granules which takes place thanks to its C-terminal low complexity domain and its RNA binding propensity (Dewey *et al.*, 2011).

1.4 The prion-like hypothesis for neurodegenerative diseases

Neurodegenerative disorders could present in sporadic and inherited forms, while only in the case of prion disorders exists the possibility of an infectious route of transmission. In fact, to date, prion diseases, or TSEs, are the unique neurodegenerative disorder showing an infectious transmissible protein species capable of recapitulating clinical disease (Moore *et al.*, 2009; Smethurst *et al.*, 2015) with no clear evidence to naturally occurring human-to-human transmission of other neurodegenerative conditions (Jucker and Walker, 2011; Holmes and Diamond, 2012). Despite this observed lack of infectivity, the high degree of misfolded protein deposition, and experimental evidence demonstrating the replication and propagation of various other neurodegenerative disease related proteins, including Aβ, tau and α-synuclein, suggests that these neurodegenerative diseases share a similar pathological mechanism with prions. These observations led to the terminology of 'prion-like' to distinguish between conditions with non-infectious characteristics, but similarities with the prion replication and propagation process (Aguzzi, 2009). The canonical model for the aggregation of misfolded proteins is the prion paradigm (Prusiner, 2013; Walker and Jucker, 2015). According to the "protein-only" hypothesis formulated in 1980 by Prusiner, which coined the term "prion" (proteinaceous infectious particle) (Prusiner, 1982), the critical pathological step in prion disorders is the conversion of the normal cellular prion protein (PrP^{C}) into its β-sheet enriched pathological conformer PrP-scrapie (PrP^{Sc}). The term scrapie derives from the name of a TSE which affects sheep and goats. Even if PrP^{Sc} has the same amino acidic sequence of PrP^{C}, it has some specific features that differentiate it from its normal counterpart, like a partial resistance to digestion with proteinase K (PK), the insolubility in non-ionic detergents and the enrichment in β-sheet content. PrP^{Sc} is able to induce other prion protein molecules to misfold and aggregate into small oligomers, protofibrils, and amyloid fibrils, perpetuating the pathological process

(Prusiner, 1998; Prusiner, 2013). Misfolded protein assemblies in NDDs other than prion disorders, have been shown to act similarly, as seeds of aggregation that can sequester their native isoforms and convert them into pathological molecules, thereby growing in size. The term "seed" indicates the smallest amount of a misfolded protein able to template the pathological conversion onto native molecules (Figure 5). Subsequent fragmentation of the aggregates and repetition of the cycle leads to the amplification of the pathological state within one cell, as well as through the nervous system *via* the release of seeds to the extracellular space, uptake by the neighboring cells and repetition of the propagation cycle (Maniecka and Polymenidou, 2015).

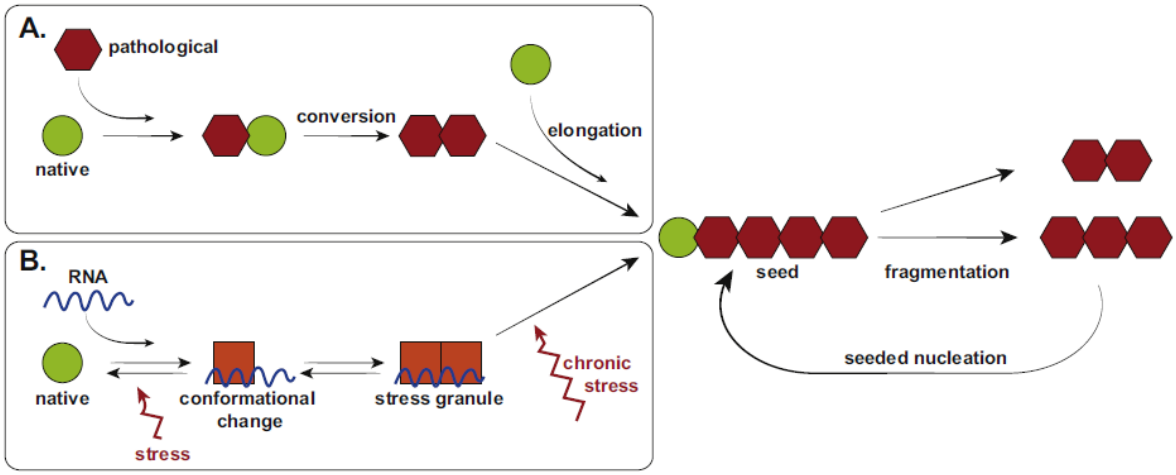

Figure 5: The prion like replication cycle. A According to the prion-like hypothesis a misfolded protein (red hexagon) is able to interact with its native isoform (green circle) and to impose on it its pathological conformation. This process can go through an elongation phase mediated by the rescue of new native protein molecules, leading to the formation of aggregates. The fragmentation of aggregates produces the seed which is the smallest amount of the pathological protein able to replicate the cycle. In the **B** panel the same concept is illustrated for an RNA-binding protein, as TDP-43. In this scenario it has been suggested that under chronic stress conditions, stress granules can represent the starting point for pathological aggregation of RNA-binding proteins. Modified from: (Maniecka and Polymenidou, 2015)

According to this concept, a misfolded protein is considered to display prion-like properties if it has seeding properties, is able to spread and propagate, to form structurally unique strains, and finally if the protein aggregates induce neurotoxicity (Smethurst *et al.*, 2015).

Among all the peculiar features of prions, one of the most intriguing is the prion strain phenomenon. Animals affected by prion diseases may develop different pathologies and clinical and biochemical outcomes could be maintained through passages in progressive animal generations. Prions, thus, are not homogeneous isomorphic particles but rather comprise a mixed population of PrP assemblies that share the ability to structurally convert other PrP molecules (Walker and Jucker, 2015). Prions are now considered to be able to adapt their conformation to changes in the context of the environment of replication (Bartz *et al.*, 2000; Morales *et al.*, 2007; Bistaffa *et al.*, 2018) and studies on synthetic prions (Legname *et al.*, 2004; Colby *et al.*, 2009) revealed that this phenomenon is replicated not only in animal models but also in an *in vitro* scenario. This process is known as either prion selection or adaptation, where a distinct PrP^{Sc} conformer present in the initial prion population with higher propensity to propagate in the new environment is able to prevail over the others during the replication process (Bistaffa *et al.*, 2018). Increasing evidence is suggesting that prion-like proteins as Aβ, α-synuclein, tau and TDP-43 do not only share the prion replication paradigm, but also this specific ability to aggregate in different conformations, i.e. strains (Sanders *et al.*, 2014; Rasmussen *et al.*, 2017; Condello *et al.*, 2018; Di Fede *et al.*, 2018; Peelaerts *et al.*, 2018; Scialo *et al.*, 2019).

1.4.1 TDP-43 prion-like properties

Several studies have demonstrated the intrinsic propensity of TDP-43 to aggregate (Johnson et al., 2009; Furukawa et al., 2011; Jiang et al., 2013) and the ability of its aggregates to act as

seeds *in vitro*, and recently, also *in vivo* (Porta et al., 2018). One of the first demonstration of TDP-43 prion-like properties comes from the work of Johnson et al. (Johnson et al., 2009), which showed an increase in the turbidity of a solution containing the full-length TDP-43 recombinant protein (recTDP-43^{FL}) under constant agitation. The same experiment was repeated using the N- and C-terminal fragments of the protein and the increase in turbidity of the solution (i.e. aggregation) was observed only in the presence of the C-terminal domain of TDP-43, confirming the crucial role of this region of the protein for its aggregation. When probed with ThT or Congo red, the final products of this reaction did not show a specific binding with these dyes, suggesting the absence of β-sheet structures in recTDP-43^{FL} aggregates (Johnson et al., 2009). Although initial pathological studies suggested that TDP-43 aggregates displayed nonamyloid structures (Neumann et al., 2007a; Kwong et al., 2008), subsequent analysis demonstrated the presence of amyloid structures in the spinal cord of a subset of ALS patients (Robinson et al., 2013). Furthermore, the use of a specific pretreatment increased the detection of amyloid positive TDP-43 inclusions in diseased tissues (Bigio et al., 2013). Another study of Furukawa et al., showed that recTDP-43^{FL} aggregates obtained *in vitro* were moderately able to bind ThT, thus, demonstrating the presence in their conformation of β-sheet structures (Furukawa et al., 2011). When analyzed at Electron Microscopy, these aggregates presented fibrillary morphology confirming what observed with the ThT-binding assay. The same group also demonstrated the seeding capacity of recombinant wild-type and mutant-insoluble TDP-43 aggregates into HEK293 cells under TDP-43 (with a C-terminal His-tag; TDP-43-HA) over-expressing conditions. The synthetic aggregates were able to seed the fibrillization of endogenous TDP-43-HA, even if there was no evidence of hyperphosphorylation of the aggregated intracellular protein, as it occurs in ALS and FTLD-TDP diseased brains (Furukawa et al., 2011). A crucial study for the demonstration of the seeding ability of TDP-43 aggregates was performed in 2013 by Nonaka and colleagues. This

group introduced human TDP-43 aggregates collected from ALS and FTLD-TDP diseased brains into normal or TDP-43 over-expressing SH-SY5Y cells. Only cells which were over-expressing the protein and that were treated with the brain extract containing the pathological TDP-43 aggregates showed the presence of bands of the hyperphosphorylated pathological protein at western blot analysis. They also demonstrated that pathological aggregates were toxic to cells, probably *via* an impairment of the cellular proteasome system and that the observed seeding reaction was time-dependent (i.e. bands appeared and increased in their intensity after the third day post-infection) and "self-templating" (Nonaka et al., 2013). The self-templating term refers to the observation that the western blot banding pattern of the sarkosyl-insoluble fraction of the affected cells mostly corresponded to the one of the pathological protein extracted from the brain used as seed. The seeding activity of pathological diseased brain extracts was confirmed by another group in a murine motor-neuron like cell line (NSC-34) under TDP-43 over-expressing conditions (Smethurst et al., 2016). Recently, a new method for the extraction of the sarkosyl-insoluble fraction from FTLD-TDP diseased brains allowed a better characterization of the obtained extracts (Laferriere et al., 2019). Laferriere and colleagues showed that aggregates associated with specific histopathological subtypes present differences in terms of dimension, density, morphology, biochemical properties and seeding capacity, supporting the concept of the existence of TDP-43 strains (see next paragraph).

Since the formation of stress granules (SGs) and the propensity of TDP-43 to phase separate (see also section 1.3.1) are considered as potential triggers for TDP-43 pathological aggregation they represent an increasingly important area of interest. Two recent studies investigated the relation between phase separation, SGs and TDP-43 aggregation, confirming that TDP-43 aggregates in cells evolve indeed from phase separated cytoplasmic inclusions, but that their formation is independent from SGs and they are devoid of RNA molecules (Gasset-Rosa et al., 2019; Mann et al., 2019). In their study, Mann and colleagues also observed that RNA

oligonucleotides, composed of TDP-43 target sequences, prevent the formation of pathological inclusions and rescue their neurotoxicity (Mann et al., 2019). To complicate this scenario, a contemporary study, conversely observed that SGs can represent the starting substrate for ALS/FTD-like TDP-43 pathological aggregates in cells (Zhang et al., 2019). These conflicting results suggest that other studies are needed to further elucidate these mechanisms and their role in pathology and that more than one event could participate in the process. Finally, Porta and colleagues, provided the first demonstration of *in vivo* spreading of TDP-43 pathology (Porta et al., 2018). They showed that intracerebral injection of biologically active pathogenic FTLD-TDP seeds into transgenic mice expressing cytoplasmic human TDP-43 and also non-transgenic mice, led to the induction of de novo TDP-43 pathology. Moreover, this group showed that TDP-43 pathology progressively spreads throughout the brain in a time-dependent manner, supposedly, via the neuroanatomic connectome (Porta et al., 2018).

1.4.2 TDP-43 strains

As for TSEs, also ALS displays different phenotypes, as for instance the predominant involvement of upper or lower motor neurons, the clinical onset involving spinal or bulbar muscles and, as already mentioned, the association with cognitive impairment in a continuum with FTD (Strong and Yang, 2011). FTD, for its part, can also present with the impairment of different cognitive abilities with predominant behavioral or language impairment (Irwin *et al.*, 2015). Furthermore, according to neuropathological examination, FTLD-TDP can be classified in different histopathological subtypes related to the shape and distribution of TDP-43 positive lesions (Lee *et al.*, 2017). All these observations led to the speculation that different conformations or ‘strains’ of misfolded TDP-43 might be responsible for the wide variety of different clinical ALS/FTD phenotypes associated to a specific strain-related distribution in

preferential CNS areas. The hypothesis of the existence of different TDP-43 aggregated species in the CNS of FTLD-TDP subjects is corroborated by the fact that there is a specific western blot banding pattern associated with each histopathological subtype, thus, suggesting different biochemical properties and conformation of the pathological aggregated TDP-43 (Nonaka and Hasegawa, 2018). Another proof in this direction was provided by the seeding experiment performed by Nonaka et al. using SH-SY5Y cells in which it was demonstrated that aggregates associated with a predominant histopathological subtype, were able to template the same biochemical properties (i.e. the same specific western blot banding pattern) on the endogenous wild-type TDP-43 protein (Nonaka *et al.*, 2013). Shimonaka et al., used TDP-43 aggregates obtained by the *in vitro* fibrillization of different C-terminal TDP-43 peptides to transduce cells expressing wild-type or mutant TDP-43 protein. They showed that the sarkosyl-insoluble fraction of these cell lysates contained specific phosphorylated TDP-43 CTFs and trypsin-resistant bands, suggesting that the templated aggregation of TDP-43, induced by different peptides, produced various types of TDP-43 pathologies (i.e., the peptides appeared to act like prion strains) (Shimonaka *et al.*, 2016). Furthermore, pathological TDP-43 brain extracts demonstrated different "infectivity" when injected in susceptible mice and, when tested in a cellular-based assay, FTLD-TDP-*GRN* lysates showed the highest seeding activity, followed by FTLD-TDP-*C9orf72* and sporadic FTLD-TDP cases (Porta *et al.*, 2018). A further support for the presence of different TDP-43 conformers in patient-derived brain tissues was provided by Laferriere and colleagues which observed that pathological forms of TDP-43 isolated from patients with distinct FTLD-TDP subtypes display distinct features, including their size, density, shape, proteolytic resistance and, most importantly, different neurotoxicity and seeding ability. Interestingly, the toxicity and seeding efficiency correlated with disease duration of the originating patient, suggesting that aggregates specific features may determine the clinical phenotype (Laferriere *et al.*, 2019). All the above-mentioned studies seemingly point toward a

consensus regarding the presence of TDP-43 strains in FTLD-TDP and ALS patients which could potentially explain the high degree of clinical and pathological heterogeneity in these disorders.

1.5 TDP-43 as a disease biomarker

Both ALS and FTD lack treatments able to interfere with the underlying pathological process. The progression of the neurodegenerative process determines a continuous and relentless clinical deterioration leading, ultimately, to death and severe cognitive impairment, respectively (Irwin *et al.*, 2015; Masrori and Van Damme, 2020). The possibility to identify TDP-43 pathology is of utmost importance in the context of targeted drug development and clinical trials design. In fact, the high failure rate of clinical trials for neurodegenerative diseases could be explained, at least in part, by the high degree of pathological heterogeneity of these disorders. A drug potentially effective on a specific pathological subset (e.g. ALS or FTD linked to TDP-43 deposition) would have no beneficial outcomes on a different subtype (e.g. ALS with SOD-1 deposition or FTD with tau aggregates). Another potential cause of clinical trials failure could be related to the timing of enrollment. The lack of early diagnostic tools, in fact, imposes the enrollment of patients in advanced clinical phases, characterized by relevant and potentially permanent neural damage. The irreversible nature of the advanced degenerative process would, in fact, imped the observation of clinical and/or laboratory improvements, deriving from a potentially effective drug or intervention. In this scenario, accurate and early detection of TDP-43 pathology is a key element to select a specific subset of ALS and FTD patients (i.e. the ones with TDP-43 pathological accumulation in the CNS) and to enroll them in clinical trials in the earliest disease phase. Pre-symptomatic identification would grant the largest therapeutic window for disease-modifying drugs. Once identified, a consistent

biochemical marker could also permit to monitor disease progression and to evaluate the effect of specific treatments.

So far, the attempts to exploit TDP-43 as a disease biomarker in patient-derived body fluids brought inconclusive data (Feneberg *et al.*, 2018). Studies on the quantification of TDP-43 isoforms in the CSF and plasma of ALS/FTLD patients, in fact, reported contradictory results. Despite one study reported higher TDP-43 levels in CSF and plasma of FTD patients carrying the C9orf72 expansion or *GRN* mutations compared to a more randomly selected FTD patient cohort and controls (Suarez-Calvet *et al.*, 2014), other two studies observed opposite results (Noto *et al.*, 2011; Kuiperij *et al.*, 2017). Data collected by these last two studies suggested that, as for Aβ in AD, the accumulation of TDP-43 in the CNS leads to decreased levels of the circulating protein. Another group, despite detecting higher levels of the phosphorylated form of full-length TDP-43 in the CSF of ALS/FTD patients, observed the same immunoreactivity at around 45 kDa also in disease controls (Steinacker *et al.*, 2008), leaving some degree of uncertainty in the interpretation of the result. These discrepancies can probably be explained by several limiting factors: i) the quantification of TDP-43 and even more of its phosphorylated form(s) in the CSF could be hampered by very low concentrations of TDP-43 pathological species; ii) the activity of low binding affinity antibodies could be decreased in the presence of high levels of immunoglobulines and albumin; iii) commercially available antibodies, restricted to a specific peptide region or phosphorylation site, may only partially recognize all pathological TDP-43 circulating species; iiii) the potentially high level of cross-reactivity between physiological and pathological TDP-43 molecules could limit the specificity of standard techniques in differentiating between normal or pathological TDP-43 products.

For the afore-mentioned reasons, the use of novel technologies, as the real time quaking induced reaction (RT-QuIC), represents an alternative approach able to overcome all these limitations related to the use of antibody- and quantification-based assays. For its relevance to this thesis,

the basis of the RT-QuIC technique functioning and its applications in the field of prion and prion-like protein detection will be described in the next paragraph.

1.6 The real time quaking induced conversion reaction

The RT-QuIC technology combines several aspects of the amyloid seeding assay (ASA) (Colby *et al.*, 2007), such as intermittent shaking, the use of a recombinant protein as a substrate, the ThT readout and native conditions of standard quaking-induced conversion (s-QuIC) (Atarashi *et al.*, 2008). This technique exploits a specific feature of Thioflavin T (ThT). ThT is a dye which undergoes a fluorescence shift upon binding to amyloid beta-sheet enriched fibers, from 342/430 to 442/482 nm excitation/emission maxima, while it does not fluoresce in the absence of amyloid fibers. The kinetics of *in vitro* amyloid formation (i.e. beta-sheet enriched structures) is usually stereotyped and composed of an initial lag phase in which the monomeric protein, (i.e. the substrate of the reaction) starts to nucleate to form multimeric species, in a process characterized by a slow kinetics. In this phase no detectable amyloid is yet present. After the solution is nucleated there is a fast growth of amyloid fibers, that eventually plateau when the soluble substrate pool has been depleted (Figure 6). When added to a fresh pool of soluble protein, fragmented amyloid fibrils (the so-called seed) can anticipate the lag phase, facilitating rapid amyloid formation, a phenomenon known as seeding reaction. (Colby *et al.*, 2007). The reaction is exposed to the desired experimental conditions in terms of shake and rest protocols, reaction buffer and temperature. All the process takes place in a shaker which is also a fluorescence reader, so the over-time recorded fluorescence of the ThT dissolved in the reaction is a reliable indirect reporter of conformational changes/aggregation of the substrate.

In the last years, this technology has been exploited as an ultrasensitive diagnostic tool for the detection of prion and prion-like pathological aggregates in patient-derived tissues and body

fluids (Salvadores *et al.*, 2014; Orru *et al.*, 2015; Fairfoul *et al.*, 2016; Bongianni *et al.*, 2017; Franceschini *et al.*, 2017; Groveman *et al.*, 2018).

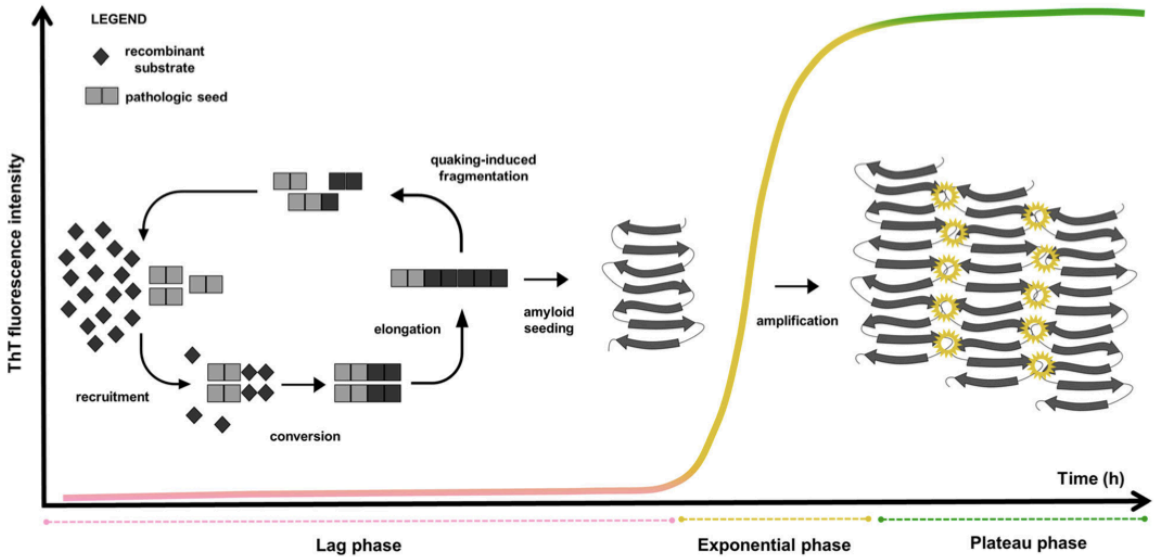

Figure 6: Schematic representation of the RT-QuIC technology. The RT-QuIC reaction may be divided into temporal stages: the lag phase, the exponential phase and the plateau phase. The lag phase represents the time required for the monomeric protein (i.e. the substrate of the reaction) to start to nucleate and form multimeric species in a process characterized by a slow kinetics. After the solution is nucleated there is a fast growth of amyloid fibers (exponential phase) that eventually plateau when the soluble substrate pool has been depleted. ThT dissolved in the reaction (yellow circles) emits fluorescence upon binding to beta-sheet fibers, acting as an indirect reporter of the aggregation of the substrate From: (Candelise *et al.*, 2020).

If a patient-derived sample contains the pathological seed, when added to the reaction it will facilitate the nucleation of the substrate, leading to an anticipation of the lag phase (i.e. will induce a seeding reaction). This seeding process could be homologous or heterologous. Homologous seeding has been reported for many of the proteins implicated in NDDs and is considered the mechanism by which the misfolded prion protein acts as an infectious agent to propagate prion diseases. Heterologous seeding, also known as "cross-seeding," occurs when oligomers composed by one misfolded protein can promote the polymerization of a different

protein substrate (Morales *et al.*, 2013). Despite heterologous seeding has been documented *in vitro* in specific settings, its role in pathology is still a matter of debate (Morales *et al.*, 2013). Regarding heterologous seeding, it should be underlined that, when optimizing an RT-QuIC assay with diagnostic purposes it is mandatory to develop a specific setting which reduces the most, and ideally abolishes, the possibility of cross-seeding, in order to minimize the risk of false positive results. Recently, RT-QuIC *ante-mortem* prion detection has proved as a robust technique for prion amplification (Orru *et al.*, 2015; Fairfoul *et al.*, 2016; Bongianni *et al.*, 2017; Franceschini *et al.*, 2017; Groveman *et al.*, 2018). RT-QuIC showed the ability to detect prions in several peripheral tissues of patients with different forms of prion diseases (Orru *et al.*, 2014; Orru *et al.*, 2015; Bongianni *et al.*, 2017; Franceschini *et al.*, 2017), misfolded Aβ oligomers in the CSF of patients with AD (Salvadores *et al.*, 2014), α-synuclein oligomers in the CSF of patients with PD and Lewy body dementia (Fairfoul *et al.*, 2016; Shahnawaz *et al.*, 2017; Groveman *et al.*, 2018; van Rumund *et al.*, 2019; Shahnawaz *et al.*, 2020) and tau in the CSF of patients with Pick's disease (Saijo *et al.*, 2017). Despite TDP-43 displays prion-like properties (Johnson *et al.*, 2009; Furukawa *et al.*, 2011; Jiang *et al.*, 2013; Nonaka *et al.*, 2013; Smethurst *et al.*, 2016; Porta *et al.*, 2018; Laferriere *et al.*, 2019), to date, the RT-QuIC technology has not yet been adapted to this protein.

CHAPTER II

2. AIMS OF THE STUDY

i) The first aim of this study was to set a reliable protocol for the production of both the full-length and the aggregation-prone C-terminal fragment of human TDP-43, in order to use them as substrates for the development of the TDP-43 RT-QuIC reaction.

One of the main limitations in the development of a TDP-43 RT-QuIC so far, has been represented, indeed, by the lack of standardized protocols for the production of high amounts of soluble recombinant TDP-43.

ii) The main aim of our project was to adapt the RT-QuIC technique to the recombinant TDP-43 substrates and to exploit this technology for the detection of pathological TDP-43 species in the CSF of ALS and FTD patients.

Our objective was to identify the best conditions for the aggregation of the TDP-43 substrate and once optimized, to investigate the possibility to use the TDP-43 RT-QuIC technology as a diagnostic tool for ALS and FTD patients.

iii) Our last objective was to perform a preliminary evaluation of the seeding properties of the *in vitro* obtained TDP-43 synthetic aggregates in a cellular model, in order to evaluate their ability to recapitulate ALS/FTD TDP-43 pathology.

The TDP-43 RT-QuIC could be exploited not only as a powerful drug screening and diagnostic tool but could also be a very helpful instrument to further elucidate TDP-43 prion-like features.

CHAPTER III

3. MATERIALS AND METHODS

3.1 Recombinant full-length and truncated TDP-43 production

The pET-11a plasmid containing human TDP-43 (HuTDP-43(1-414)) coding sequence was purchased from GenScript. The truncated construct (HuTDP-43(263-414)) was obtained by deleting the DNA region encoding for HuTDP-43 fragment 1-262 using mutagenesis. PCR was carried out using site-directed mutagenesis kit (Agilent) with the following primers: 5'-ttaagaaggagatatacatatgaaacacaacagcaaccgtcagc-3', 5'-gctgacggttgctgttgtgtttcatatgtatatctccttcttaa-3'. The protein production protocol was the same for both full-length and the truncated form of the protein. The construct was expressed in Escherichia coli BL21 (DE3) cells (Stratagene). Freshly transformed overnight culture was inoculated into Luria Bertani medium with 100 μg/mL ampicillin. At 0.8 OD600, protein expression was induced with isopropyl β-D-1 thiogalactopyranoside (IPTG) to a final concentration of 1 mM. Following overnight incubation at 37°C, cells were lysed by a homogenizer (PandaPLUS 2000) and inclusion bodies were washed in a buffer containing 25 mM Tris-HCl, 5 mM ethylenediaminetetraacetic acid (EDTA), 0.8% TritonX100, (pH 8) and then in bi-distilled water (ddH2O) several times. Inclusion bodies containing HuTDP-43(1-414) or HuTDP-43(263-414) were dissolved in 5 volumes of 8 M guanidine hydrochloride (GdnHCl), loaded onto pre-equilibrated HiLoad 26/60 Superdex 200-pg column, and eluted in 25 mM Tris–HCl (pH 8), 5 mM EDTA, and 5 M GdnHCl at a flow/rate of 1.5 mL/min. Protein refolding was performed by dialysis against different refolding buffers (10 mM PBS (pH 8) for the full-length protein; 10 mM PBS (pH 8) or 25 mM Tris-HCl (pH 8) for the truncated

fragment) using a Spectrapor membrane. Purified proteins were analyzed by SDS-PAGE gel electrophoresis under reducing conditions and Western blot.

3.2 Electrophoretic Mobility Shift Assay (EMSA)

A specific sequence of RNA oligonucleotides, termed AUG12 RNA, 5′-GUGUGAAUGAAU-3′, was purchased from Sigma-Aldrich. Depending on the different experimental setting 12.5 µM of AUG12 RNA was mixed with 12.5 µM (1:1 molar ratio), 25 µM (1:2 molar ratio), 62.5 µM (1:5 molar ratio) of monomeric HuTDP-43, 37.5 µM (1:3 molar ratio) of HuTD-43 *in vitro* obtained aggregates or 12.5 µM (1:1 molar ratio) and 62.5 µM (1:5 molar ratio) of Bovine Serum Albumine (BSA), as a control. Binding reactions (20 µL) were incubated in water at room temperature (RT) for 20 min before loading onto an Agarose gel (1%) in 1X Tris-acetate-EDTA. Gels were run at 100–120 volts for 45 minutes at 4°C.

3.3 Brain homogenates (BH) collection e preparation

Post-mortem frozen frontal cortices samples of patients with a confirmed neuropathological diagnosis of FTLD-TDP associated with *C9orf72* expansion (n=1), FTLD-TDP with mutation in the *GRN* gene (n=1), FTLD-TDP with unknown genetic background (n=1) and of a normal control brain (n=1) were collected. Brain samples (0.5 g) were homogenized as previously described with some modification (Nonaka *et al.*, 2013). Briefly, samples were homogenized in 2.5 mL of homogenization buffer (HB: 10 mM Tris-HCl, 0.8 M NaCl, 1 mM EDTA, 1 mM dithiothreitol (DTT), 1X protease and phosphatase inhibitor cocktail tablets (Roche), pH 7.5). Benzonase (Sigma) was added (0.25 µL) to aliquots of 500 µL for each of the lysates, which were then incubated in constant shaking (400 rpm) for 10 min at 37°C. After this, Sarkosyl was

added to each aliquot (final concentration: 1%) and samples were then incubated for 20 min at 37°C under shaking (400 rpm). Ethanol was added to a final concentration of 20% and samples were incubated in constant shaking (400 rpm) for 10 min at 37°C. Samples were centrifuged at 150,000 x g for 60 min at RT. Supernatants were discarded, and pellets were suspended in 300 µL PBS by sonication and centrifuged at 150,000 x g for 60 min at RT. The resulting pellets were suspended in 50 µL of ddH2O by sonication and diluted at 10^{-3} volume/volume in ddH2O.

3.4 CSF samples collection and study population

Informed consent was given by all study participants or their next of kin. CSF samples were collected by lumbar puncture (LP) following a standard procedure, centrifuged at 1000 x g for 10 min and stored in polypropylene tubes at −80 °C, until analysis. Table 1 summarizes the characteristics of the study population. We retrospectively analyzed CSF samples from a total of 36 ALS/FTD patients (21 males and 15 females) harboring a pathological mutation in one of the genes known to be related to CNS TDP-43 deposition (i.e. *C9orf72*, *TARDBP*, *GRN*) (see Supplementary Table 1). Samples were provided by several Italian institutions and specifically from: the Department of Neuroscience, Rehabilitation, Ophthalmology, Genetics, Maternal and Child Health, University of Genoa, IRCCS Ospedale Policlinico, San Martino, Genoa; the "Rita Levi Montalcini" Department of Neuroscience, University of Turin, Turin; the Fondazione IRCCS Istituto Neurologico Carlo Besta, Unit of Neurology 5 and Neuropathology, Milan; the Department of Neurology and Laboratory of Neuroscience, IRCCS, Istituto Auxologico Italiano, Milan; the Molecular Markers Laboratory, IRCCS Istituto Centro San Giovanni di Dio Fatebenefratelli, Brescia; the Department of Clinical and Experimental Sciences, Neurology Unit, University of Brescia, Brescia and from the Clinical Unit of Neurology, Department of Medicine, Surgery and Health Sciences, Neurology Unit, University Hospital and Health

Services of Trieste, University of Trieste, Trieste. We collected 19 CSF samples from patients with a *C9orf72* expansion, three from patients with a *TARDBP* mutation and 14 *GRN* mutated subjects. The *C9orf72* population was composed of 10 ALS patients (two of them with associated signs of cognitive decline, not reaching criteria for FTD diagnosis), eight FTD affected subjects and one subject with an AD-like phenotype (all of them without signs of motor neuron involvement). All *TARDBP* mutated subjects were clinically diagnosed as ALS. ALS and FTD diagnoses were made according to current diagnostic criteria (Brooks *et al.*, 2000; Rascovsky *et al.*, 2011). Among the *GRN* population one sample derived from a pre-symptomatic subject without any clinical sign. Except for this subject, all patients in the *GRN* population presented with cognitive impairment. Ten *GRN* patients were classified as FTD and more specifically, eight were diagnosed as behavioral variant FTD (bv-FTD) and two as agrammatic variant of primary progressive aphasia (avPPA) according to current redefined clinical criteria (Gorno-Tempini *et al.*, 2011; Rascovsky *et al.*, 2011). Three *GRN* patients were not diagnosed as FTD. One had a clinical diagnosis of cortico-basal syndrome (CBS), one of mild cognitive impairment (MCI) and one was diagnosed as AD according to current clinical diagnostic criteria (McKhann *et al.*, 2011; Armstrong *et al.*, 2013). We also collected CSF from 27 age-matched control subjects (14 males and 13 females), which underwent a lumbar puncture to exclude a neurological disease. In none of these cases was the suspected disease, ALS, FTD, or any other neurodegenerative disorder. Leukocyte count, glucose, total protein, blood pigments, lactate, and oligoclonal IgG bands were all normal in the analyzed CSF.

3.5 *In vitro* generation of recombinant human TDP-43 aggregates

In vitro aggregation reactions of human TDP-43 were performed in 200 µL of reaction mix in black, clear-bottom, 96-well microplates. The reaction mix contained 10 mM PBS at pH 6.8, 5

mM DTT, 100 mM NaCl, 50 μM thioflavin-T (ThT), 0.002% of sodium dodecyl sulfate (SDS) and 2 mg/mL of HuTDP-43. After sealing, the plate was incubated at 40 °C, over a period of 50 hours with intermittent cycles of shaking (60 s, 400 rpm, double-orbital) and rest (60 s). For HuTDP-43(263-414) aggregation, the reaction mix contained 10 mM PBS at pH 7.8, 100 mM NaCl, 10 μM ThT, 0.002% of SDS and 0.2 mg/mL of HuTDP-43(263-414). After sealing, the plate was incubated at 40 °C, over a period of 24 hours with intermittent cycles of shaking (60 s, 400 rpm, double-orbital) and rest (60 s). All reactions were performed in a FLUOstar OMEGA reader (BMG Labtech, Germany) and fluorescence intensity, expressed as relative fluorescence units (RFU), was taken every 30 minutes using 450 ± 10 nm (excitation) and 480 ± 10 nm (emission) wavelengths and a gain of 1,000. All solutions were filtered before use with 0.22 μm sterile filters. Recombinant proteins were subjected to 2 hours of centrifugation at 186,000 g at RT before their use in the reaction. The addition of a 3-mm glass bead (Sigma) was required to sustain protein aggregation. The final product of these reactions was collected by ultracentrifugation at 100,000 x g for 1 hour and suspended by sonication in the same starting volume of ddH2O and used as synthetic seed. Protein aggregates were analyzed by atomic force microscopy.

3.6 TDP-43 RT-QuIC optimization

All RT-QuIC reactions were performed in 200 μL of reaction mix in black, clear-bottom, 96-well microplates. To optimize the reaction for HuTDP-43 and its truncated fragment HuTDP-43(263-414) we used different experimental protocols. The RT-QuIC reaction mix contained 10 mM PBS at pH 6.8, 5 mM DTT, 100 mM NaCl, 25 μM ThT, 0.002% of SDS and 1 mg/mL of HuTDP-43. After sealing, the plate was incubated at 40 °C, over a period of 50 hours with intermittent cycles of shaking (60 s, 400 rpm, double-orbital) and rest (60 s). For HuTDP-

43(263-414) aggregation the reaction mix contained 10 mM PBS at pH 7.8, 100 mM NaCl, 10 µM ThT, 0.002% of SDS and 0.2 mg/mL of HuTDP-43(263-414). After sealing, the plate was incubated at 40 °C, over a period of 24 hours with intermittent cycles of shaking (60 s, 400 rpm, double-orbital) and rest (60 s). We also optimized another reaction condition with HuTDP-43(263-414) in terms of reaction buffer and shaking protocol. The reaction buffer was changed as follows: 40 mM Tris (pH 8), 0.5 M guanidine hydrochloride (GdnHCl) (pH 8), 10 µM ThT, 0.002% of SDS and 0.05 mg/mL of HuTDP-43(263-414). After sealing, the plate was incubated at 40 °C, over a period of 50 hours exposed to 15 seconds of shaking every 30 minutes at 100 rpm (double-orbital). Reactions were performed in a FLUOstar OMEGA reader (BMG Labtech, Germany) and the fluorescence intensity, expressed as relative fluorescence units (RFU), was taken every 30 minutes using 450 ± 10 nm (excitation) and 480 ± 10 nm (emission) wavelengths, with a bottom read and a gain of 1,000. All solutions were filtered before use with 0.22 µm sterile filters. Recombinant proteins were subjected to 2 hours of centrifugation at 186,000 x g at RT before their use in the reaction. The addition of a 3-mm glass bead (Sigma) was required to sustain protein aggregation. Reactions were seeded with 20 µL of 10^{-3} diluted BH samples.

3.7 CSF TDP-43 seeds detection with RT-QuIC

For CSF TDP-43 seeds detection 6 µL of each CSF sample were added to 194 µL of reaction mix in black, clear-bottom, 96-well microplates. Samples were tested in triplicate. To test CSF samples, we used our optimized protocol for HuTDP-43(263-414). The RT-QuIC reaction mix contained 40 mM Tris at pH 8, 0.5 M GdnHCl (pH 8), 10 µM ThT, 0.002% of SDS and 0.05 mg/mL of HuTDP-43(263-414). All solutions were filtered before use with 0.22 µm sterile filters. Recombinant HuTDP-43(263-414) was centrifuged 2 hours at 186,000 x g at RT to

remove preformed aggregates before its use in the reaction. After sealing, the plate was incubated in a FLUOstar OMEGA reader (BMG Labtech, Germany) at 40 °C, over a period of 72 hours. Every 30 minutes the reaction was exposed to 15 seconds of shaking at 100 rpm (double-orbital). The fluorescence intensity of the reaction was taken every 30 minutes using 450 ± 10 nm (excitation) and 480 ± 10 nm (emission) wavelengths, with a bottom read and a gain of 1,000. The addition of a 3-mm glass bead (Sigma) was required to sustain protein aggregation. A CSF sample was considered positive in a single experiment if two out of three well reached a defined RFU threshold (five times their starting fluorescence value) before a time threshold of 56.6 hours (see paragraph 3.11). To be considered as a definite positive, each sample had to test positive in two out of three independent experiments. To investigate the detection power of our technique we serially diluted (till 10^{-6}) the in vitro obtained HuTDP-43(263-414) aggregates in a previously screened true negative CSF sample which was analyzed with the same protocol used to asses all other CSF samples.

3.8 Immune-depletion of TDP-43 species

For each sample, 50 µL of resuspended PureProteome Protein A magnetic beads (MerkMillipore-LSKMAGA02) were used. After three washes with 500 µL PBS 1X 0.1% Tween 20, beads were resuspended in 100 µL of PBS 1X 0.1% Tween 20, and added to a cocktail composed of 10 µg of rabbit polyclonal anti-C-terminal (Sigma-Aldrich-T1580) and 10 µg of rabbit polyclonal anti-N-terminal (Sigma-Aldrich SAB4200006) TDP-43 antibodies. After 30 minutes of incubation at RT in constant agitation the buffer was discarded and 60 µL of each sample were incubated with the antibody-coated beads for 24 hours at 4°C with constant mixing. Depleted samples were subsequently analyzed with the optimized TDP-43 RT-QuIC protocol.

3.9 *In vitro* generation of recombinant human α-synuclein and tau K18 aggregates

Recombinant full-length human α-synuclein (α-syn) and tau K18 fragment were provided from collaborators in our group. Expression and purification of recombinant tau K18 fragment and of full-length α-syn were performed as previously described (Barghorn *et al.*, 2005; Huang *et al.*, 2005). In vitro fibrillization reactions were performed at 37°C with intermittent cycles of shaking (50 s, 400 rpm, double-orbital) and rest (10 s) in a FLUOstar OMEGA reader (BMG Labtech, Germany). Newly formed aggregates were pelleted by ultracentrifugation (186,000 x g for 1 hour at 4°C) and resuspended in sterile ddH2O. Before their use, aliquots were sonicated for 3 minutes in an ultrasonic bath (Branson 2510).

3.10 Atomic force microscopy analysis

TDP-43 in vitro generated aggregates were dialyzed against bi-distilled water at RT overnight and then subjected to AFM imaging. A volume of 10 µL was dropped onto freshly sliced muscovite mica (V-1) and incubated for 15 min for sample adhesion. The same volume of absolute ethanol was added allowing the drop to evaporate. The sample was left to dry at RT and subjected to AFM imaging (NT-MDT Solver-Pro) in semi-contact mode, using commercial silicon cantilevers (NSG03, NT-MDT Spectrum Instruments, <10 nm radius of curvature, spring constant of 1.74 Nm-1).

3.11 Lag phase threshold definition

We performed the RT-QuIC reaction with all control and patient samples in three separate experiments, each one in triplicate, and we collected for each well of each experiment the time needed to reach an arbitrary fluorescence threshold that we set at five times the initial fluorescence value of each well. We then calculated the median lag phase time for each triplicate and, subsequently, the median of the medians resulting from the three independent experiments (that we will call "total median time"). This procedure provided a single and informative number for each subject (i.e. the total median time). After this, we plotted the distribution of total median times and from the observation of these distributions we derived the lag phase threshold of 56.6 hours (Figure 11A). In order to address the risk of overfitting, we cross-validated our data. For a thousand times we simulated to split the dataset into a training set comprising 50% of the data, (i.e. 14 controls and 18 patients) and a testing set (i.e. the remaining 50%). For each simulation we defined the threshold based on the training set and applied it to the testing set to compute the cross-validated accuracy. To illustrate how the choice of the lag phase threshold would influence the True Positive Rate (TPR) and False Positive Rate (FPR) numbers, we built the ROC (Receiver Operating Characteristic) curve which highlights the points with the highest accuracies (Figure 11B).

3.12 Statistical analysis

For the correlation analysis between baseline patient characteristics and RT-QuIC positive results, we used different tests. For binary features, we performed Welch two-sample t-tests, for categorical baseline characteristics, we used ANOVAs, and for continuous features, both linear models and ANOVAs. All statistical analyses were conducted in R (R Core Team, 2014) and figures were produced using the package ggplot2 (Wickham, 2009). All RT-QuIC graphs

were produced with GraphPad (PRISM 7.0a) and the respective figures were generated with Inkscape 1.0.

3.13 Cell culture and transfection

SH-SY5Y cells were cultured in DMEM-F12 (GIBCO) media supplemented with 10% fetal bovine serum (FBS), 1% non-essential amino acids and 1% penicillin-streptomycin and incubated at 37 °C, 5% CO_2. SH-SY5Y cells were stably transfected with pcDNA3-EGFP (Addgene) using the Effectene Transfection Reagent kit (Qiagen), according to the manufacturer guidelines. After selection of positive clones, cells were collected and used for further experiments.

3.14 Treatment with HuTDP-43(263-414) fibrils

The final product of the HuTDP-43(263-414) RT-QuIC reaction (performed in the absence of ThT) was collected by ultracentrifugation at 186,000 x g for 1 h and suspended by sonication in sterile PBS. The sonicated material was mixed with lipofectamine and added to SH-SY5Y culture medium to a final concentration of 500 nM. After 24 or 72 h cells were processed for immunofluorescence and analyzed at the confocal microscopy.

3.14.1 Fluorescence imaging

Cells were grown on poly-L-lysine-coated coverslips for 24 h, exposed to HuTDP-43(263-414) fibrils (see paragraph above) at 500 nM concentration for 24 or 72 h before immunofluorescence analysis. Cells were fixed in 4% paraformaldehyde (20 min), washed with

PBS and permeabilized for 10 min with 0.3% Triton X-100 prior to 1 h blocking in 7% normal goat serum (NGS), 0.3% Triton X-100. Cells were incubated for 2 hours at 4°C with primary antibodies and after 3 washes with PBS incubated with the respective secondary antibodies conjugated with Alexa Fluor. Coverslips were mounted in Fluoromount-GTM (ThermoFisher Scientific) and stored at 4°C for confocal fluorescence microscopy. Images were acquired using a Nikon confocal microscope (Nikon C1). Primary antibodies: rabbit polyclonal anti-TDP-43 C-terminal (Sigma-Aldrich-T1580); rabbit polyclonal anti-TDP-43 N-terminal (Sigma-Aldrich SAB4200006) and rat monoclonal anti-phospho TDP-43 (Ser409/Ser410), clone 1D3 (Sigma-Aldrich-MABN14).

3.15 Cell vitality assay (MTT)

Cells were seeded to a concentration of $1x10^4$ in a 96-well, tissue culture-treated, clear bottom, plate (Costar). Cells were allowed to grow for 24 h at 37 °C under 5% CO_2 prior to the addition of HuTDP-43(263-414) fibrils (prepared as described above; see paragraph 3.14). TDP-43 fibrils were diluted in the cell medium to a final concentration of 500 nM. After the addition of fibrils, cells were cultured at 37 °C under 5% CO_2 for 24 h. 3-(4,5-dimethylthiazol- 2-yl)-2,5-diphenyltetrazolium bromide (MTT, SIGMA) was diluted in PBS to a working dilution of 5 mg/mL. The medium was then removed, and cells were incubated with the MTT solution for 3 hours at 37 °C under 5% CO_2. After incubation, a solution of DMSO/2- Propanol (1:1) was added to each well and the plate was kept at RT for 30 min before reading. The emission intensity was quantified using a Spectramax Gemini EM (SoftMax Pro) plate reader, excitation/emission ratio equal to 570/690 nm. MTT assays were performed in triplicate.

3.16 Standard RT-PCR and RT-qPCR analysis

Total RNA from each sample was purified using TRIzol reagent (Invitrogen) according to manufacturer instructions. The cDNA synthesis was performed using 1 μg of each RNA with 50 μM Oligo(dT)20, 10 mM dNTP mix, 5X First Strand Buffer, 0.1 M DTT, 40 U RNAse inhibitor, and 200 U SuperScript III Reverse Transcriptase (Life Technologies). PCR analysis was performed using the following primers: *POLDIP3* Fw 5'-gcttaatgccagaccgggagttg-3'; *POLDIP3* Rv 5'-tcatcttcatccaggtcatataaatt-3'; *STAG2* Fw 5'-gtatgtttacttggaaaagttcatg-3'; *STAG2* Rv 5'-tgattcatccataattgaagctgga-3'. Specific qPCR primers were designed using the online tool Primer-Blast provided by NCBI. The primer sequences were as follows: for *GAPDH* Fw 5′-cctgcaccaccaactgctta-3′ and Rv 5′-tcttctgggtggcagtggatg-3'; *TARDBP* Fw 5'-cagcttcggagagttctggg-3'; *TARDBP* Rv 5'-cagcaaaccgcttgggatta-3'. Gene expression assays were performed using iQ™ SYBR Green Supermix 2x (Bio-Rad Laboratories, Inc.), 400nM final concentration of the corresponding forward and reverse primers (Sigma) and 10 ng/μL final concentration of cDNA samples, with CFX96 Touch™ Real-Time PCR Detection System (Bio-Rad Laboratories, Inc.).

CHAPTER IV

4. RESULTS

4.1 Part I-development and optimization of the TDP-43 RT-QuIC

4.1.1 Recombinant full-length and truncated TDP-43 production

The first step in the adaptation of the RT-QuIC methodology to TDP-43 was to obtain high amounts of soluble recombinant protein to be used as the substrate for the reaction. After several trials, we optimized an efficient protocol for full-length TDP-43 (HuTDP-43) production and refolding (see paragraph 3.1 in the materials and methods chapter) (Figure 7A).

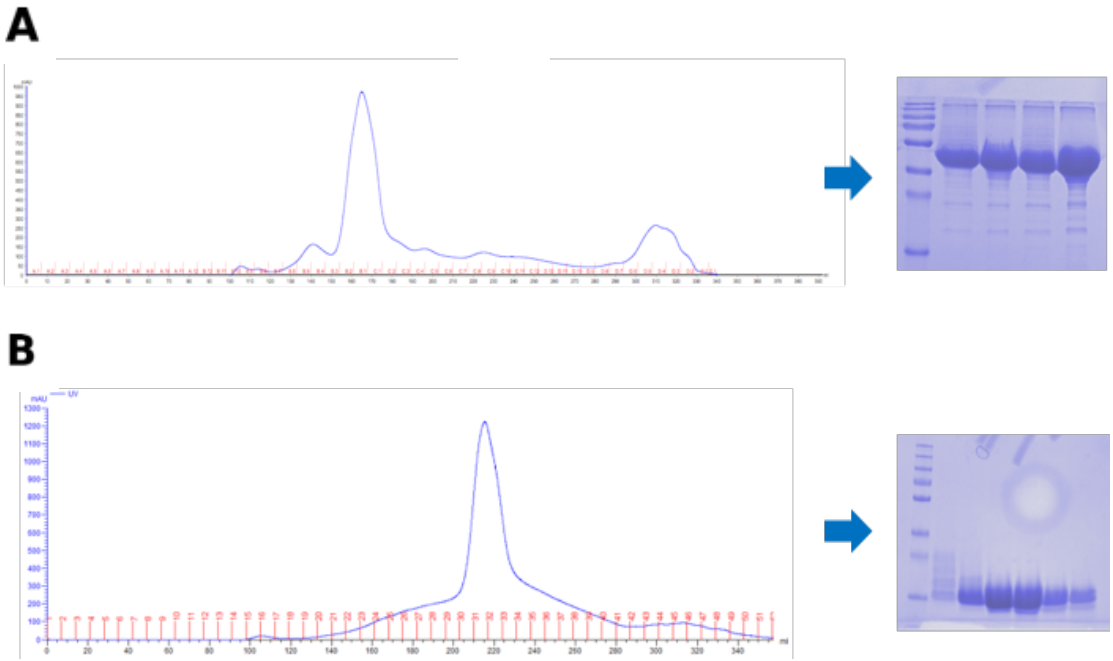

Figure 7: Protein purifications. Chromatographic plot of the purification of HuTDP-43 (**A**) and HuTDP-43(263-414) (**B**) and the corresponding SDS-PAGE of the collected fractions. Both proteins were expressed in E.Coli BL21 and obtained from inclusion bodies. Protein

purification has been performed by SEC under denaturating conditions using a Superdex HiLoad 26/60 column.

After refolding, the recombinant protein product was highly pure and devoid of signs of degradation (Figure 8A, B).

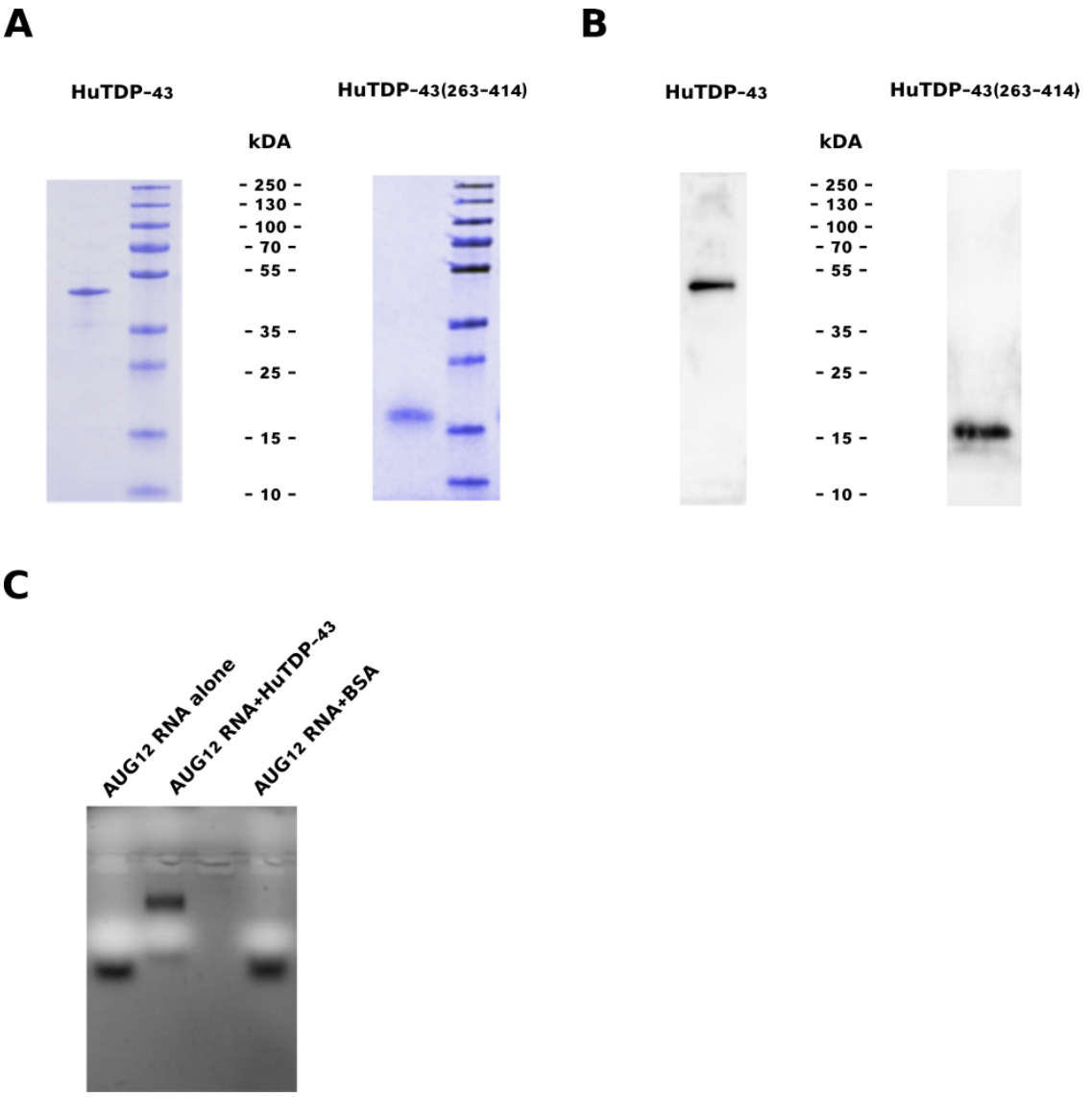

Figure 8: Characterization of purity and functionality of recombinant TDP-43. Coomassie-stained gel (**A**) and Western blot (WB) analysis (**B**) of HuTDP-43 and HuTDP-43(263-414) after the purification and refolding process. For Coomassie gel, 1 µg of recombinant proteins was loaded, while the WB was performed with 30 ng of protein products probed with a polyclonal antibody against TDP-43 C-terminal domain. **C** shows the results of

the Electrophoretic Mobility Shift Assay (EMSA): The first line corresponds to free AUG12 RNA (12.5 μM), the second one to the same amount of AUG12 RNA mixed with HuTDP-43 at a 1:1 molar ratio and the last line to AUG12 RNA mixed with Bovine Serum Albumin (BSA) at the same molar ratio, as a control.

Since the C-terminal domain of TDP-43 is known to be aggregation-prone (Saini and Chauhan, 2011; Budini *et al.*, 2012) we produced also a recombinant C-terminal fragment from amino acid 263 to the end of the protein (HuTDP-43(263-414)) (Figure 7B). Also in this case the final protein product was pure and devoid of signs of degradation (Figure 8A, B). TDP-43 is able to bind UG-rich RNA sequences thanks to its RRMs domains (Lukavsky *et al.*, 2013). To investigate the folding state and functionality of the produced recombinant HuTDP-43 we performed the Electrophoretic Mobility Shift Assay (EMSA) using as RNA probe a specific sequence of RNA oligonucleotides, termed AUG12 RNA, 5′-GUGUGAAUGAAU-3′, known to be recognized by TDP-43 with high affinity (Lukavsky *et al.*, 2013). The EMSA analysis showed that the produced recombinant product was functional in terms of its RNA-binding ability (Figure 8C).

4.1.2 Adaptation of RT-QuIC to TDP-43 amplification

Once obtained adequate amounts of human TDP-43 recombinant products, the second critical step in the adaptation of the RT-QuIC technique was to identify the best conditions for the aggregation of the substrates. Several factors were modified to improve the efficiency and reproducibility of TDP-43 RT-QuIC, such as protein concentration, temperature, pH of the reaction and shaking protocol. Figure 9A shows the aggregation kinetics profile of HuTDP-43. The aggregation curve is characterized by a lag phase of about 15-20 hours, followed by a slow and progressive increase in thioflavin T (ThT) fluorescence emission and a subsequent plateau

reached after around 30-35 hours (Figure 9A, black line). We collected the final product of this reaction and employed it as a synthetic aggregate. When the synthetic seed was added to the reaction, we observed a clear anticipation of the lag phase associated with an increase in the amount of ThT fluorescence emission (Figure 9A, green line). Interestingly, the aggregation profile observed in our experimental setting, substantially differed from those observed in previous studies where the aggregation curve of HuTDP-43 completely lacked a lag phase (Johnson *et al.*, 2009; Furukawa *et al.*, 2011; Jiang *et al.*, 2013). To characterize the aggregates used as synthetic seeds we subjected them to atomic force microscopy (AFM) analysis, observing that they mainly displayed features of amorphous aggregates, lacking fibrillary structures (Figure 9C). Next we tested the aggregation properties of the produced TDP-43 C-terminal fragment, HuTDP-43(263-414) and observed a typical prion-like aggregation kinetics (Figure 9B, black line). Compared to HuTDP-43, HuTDP-43(263-414) aggregation curve showed a shorter lag phase and higher values of ThT fluorescence emission (Figure 9). The final product of this reaction was also very efficient as synthetic seed (Figure 9B, green line). AFM analyses of HuTDP-43(263-414) aggregates differed substantially from those of HuTDP-43, presenting typical fibrillary features (Figure 9D). We considered that the different aggregation profiles of HuTDP-43 and HuTDP-43(263-414) were strictly related to the different final conformation acquired by their aggregates (Figure 9). Only a fraction of HuTDP-43 would acquire beta-sheet conformation, thus binding ThT, while HuTDP-43(263-414) is readily converted in beta-sheet enriched fibrils.

4.1.3 TDP-43 RT-QuIC optimization

To investigate which substrate (HuTDP-43 or HuTDP-43(263-414)) was more efficient to detect biological TDP-43 aggregates, we seeded the reaction with a small pool of pathological

confirmed patient-derived brain homogenates. HuTDP-43 and HuTDP-43(263-414) were both efficiently seeded by three positive BH samples, while a negative control BH at the same dilution (10^{-3}) did not affect the aggregation kinetics of the reaction (Figure 10A, B).

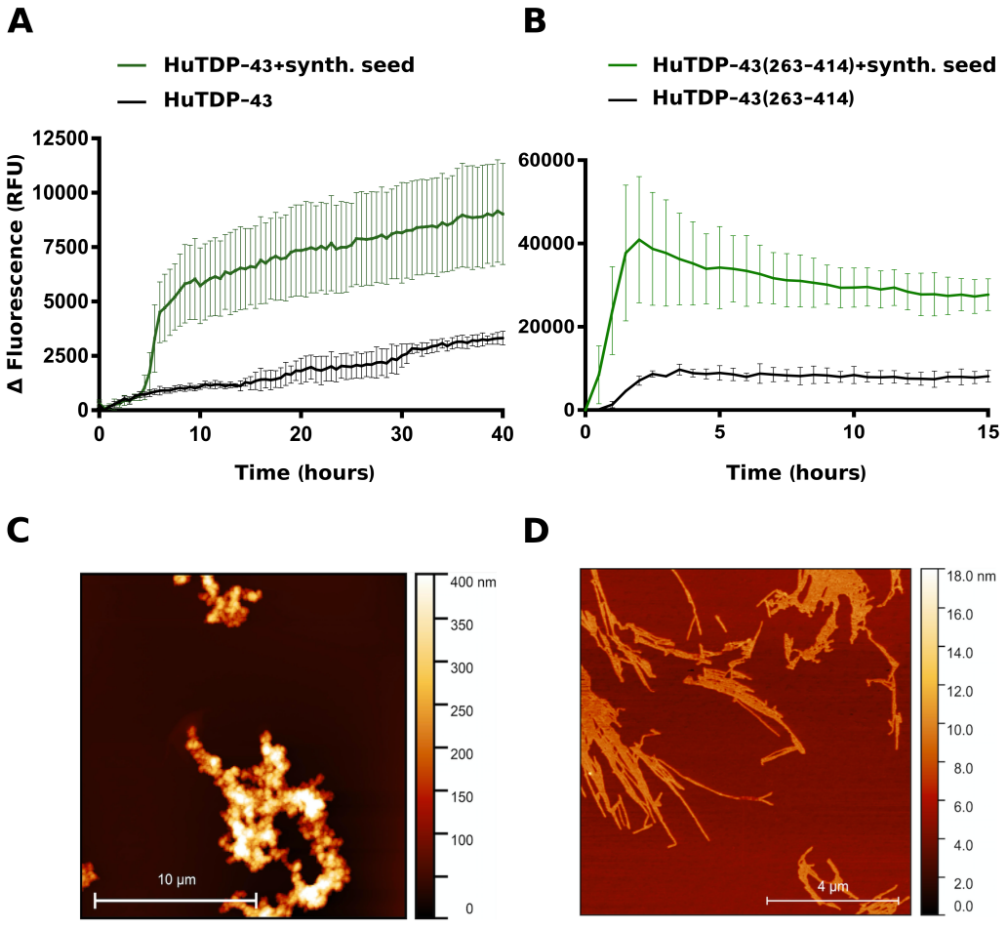

Figure 9: Aggregation kinetics of recombinant TDP-43 and AFM seeds characterization. Purified seed-free recombinant HuTDP-43 (2 mg/mL) (**A**) and HuTDP-43(263-414) (0.2 mg/mL) (**B**) were induced to aggregate by alternating cycles of 60 seconds (s) of shaking and 60 s of incubation at 40 °C (black lines). The final product of their aggregation was collected and efficiently employed as synthetic seed (green lines). ThT fluorescence is plotted against time. Each graph has a specific range of ThT fluorescence values and duration of a given reaction. The experiment was performed in triplicate and each replica was performed three times. Curves represent means for all experimental replicates and bars indicate the standard deviations (SD). **C**, **D** Atomic force microscopy (AFM) analysis of TDP-43 aggregates.

HuTDP-43 aggregates showed features of amorphous aggregates (**C**), while HuTDP-43(263-414) (**D**) acquired a fibrillary structure after aggregation.

This trial indicated that both proteins were suitable substrates for the amplification assay.

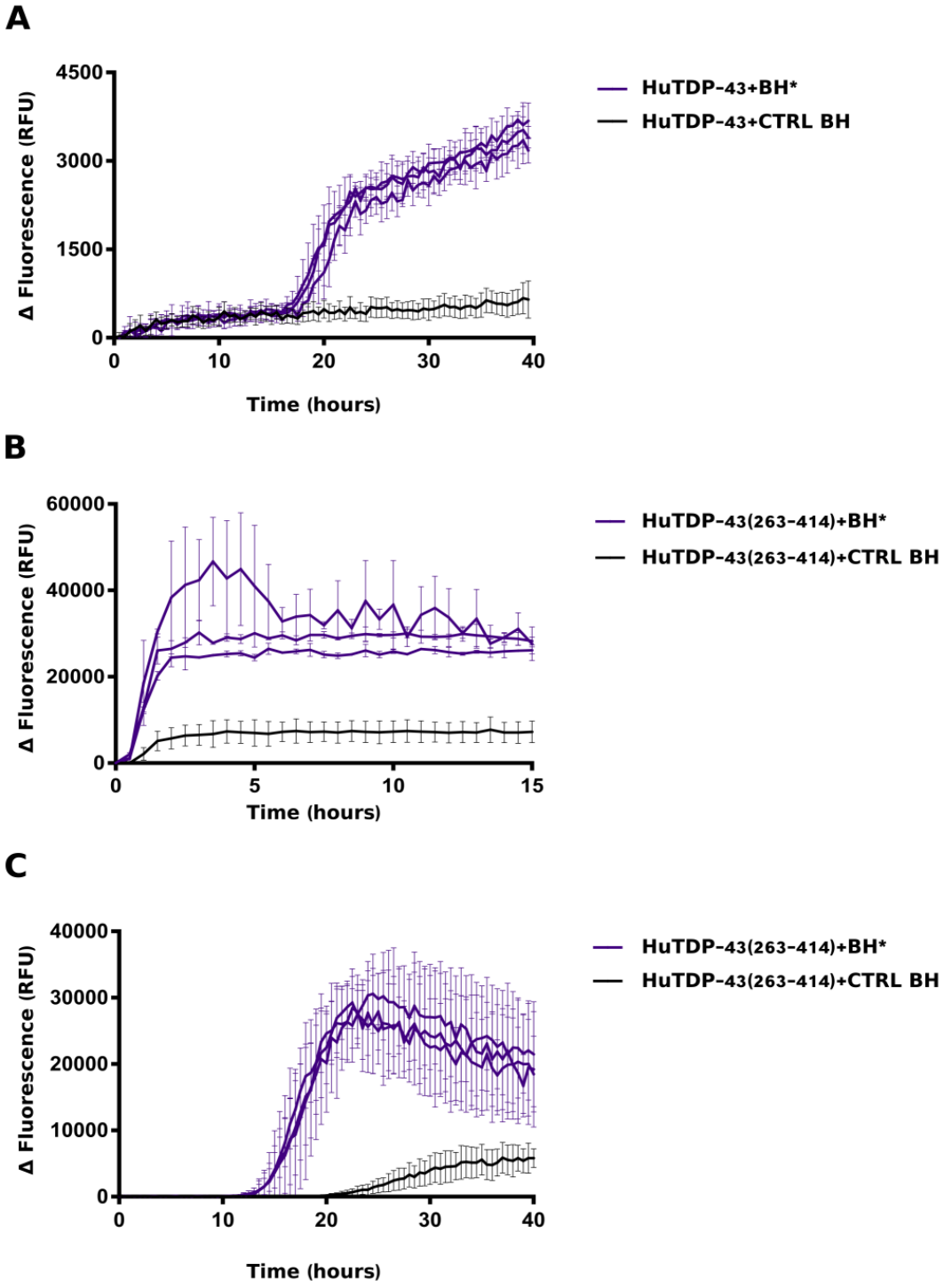

Figure 10: RT-QuIC analysis of BH samples. 20 µL of sonicated and diluted (10^{-3}) BHs collected from 3 FTLD-TDP patients (BH*, purple lines) and 1 CTRL subject (CTRL BH, black line) were added to purified seed-free recombinant HuTDP-43 (1 mg/mL) (**A**) and HuTDP-43(263-414) (0.2 mg/mL) (**B**) and analyzed by means of RT-QuIC. The reaction was exposed to 60 s of shaking and 60 s of rest. All positive BHs efficiently seeded the reaction, while the negative control BH at the same dilution (10^{-3}) did not affect the aggregation kinetics of the reaction. **C**. Optimized protocol for BH analysis using purified seed-free HuTDP-43(263-414) (0.05 mg/mL) as substrate with a different reaction buffer (no NaCl, Gdn-HCl added) and a modified protocol (shaking at 100 rpm for 15 s every 30 minutes at 40 °C). ThT fluorescence intensity was plotted against time. Each graph has a specific range of ThT fluorescence values and duration of a given reaction. The experiment was performed in triplicate and each replica was performed three times. Curves represent means for all experimental replicates and bars indicate the standard deviations (SD).

Nevertheless, since the reaction with HuTDP-43 required higher amounts of substrate, we selected HuTDP-43(263-414) as the most efficient product to perform further analyses. Another relevant point for the optimization of the TDP-43 RT-QuIC technology as a tool to detect TDP-43 seeds, was to obtain a slower aggregation profile of the substrate, to provide the optimal time window for discrimination between positive and negative samples. For this purpose, we modified the reaction buffer with the addition of guanidine hydrochloride (Gdn-HCl) and the removal of NaCl. We also reduced the amount of the HuTDP-43(263-414) substrate from 0.2 mg/mL to 0.05 mg/mL and modified the aggregation protocol (only 15 seconds of shaking every 30 minutes, at 100 rpm). After this optimization, all positive BH samples maintained their seeding activity but, as expected, with a slower aggregation kinetics (Figure 10C).

4.1.4 CSF TDP-43 seeds detection with RT-QuIC

Since our final aim was to screen CSF samples, it was also important to take into account the effect of the CSF material to the reaction. When small aliquots of CSF (control or disease) were

added to the reaction, we observed an inhibition of HuTDP-43(263-414) aggregation. This was expected, since this CSF inhibiting effect was also experienced by other groups (Shahnawaz *et al.*, 2017). For this reason, the threshold that we set to discriminate between positive and negative CSF samples, derived from the comparison between all our CSF samples (disease and control) (Figure 11), since the spontaneous aggregation of the substrate (i.e. the reaction performed with the substrate alone without addition of CSF aliquots) was not a reliable parameter (see also paragraph 3.11 in the materials and methods section for lag phase threshold definition).

A

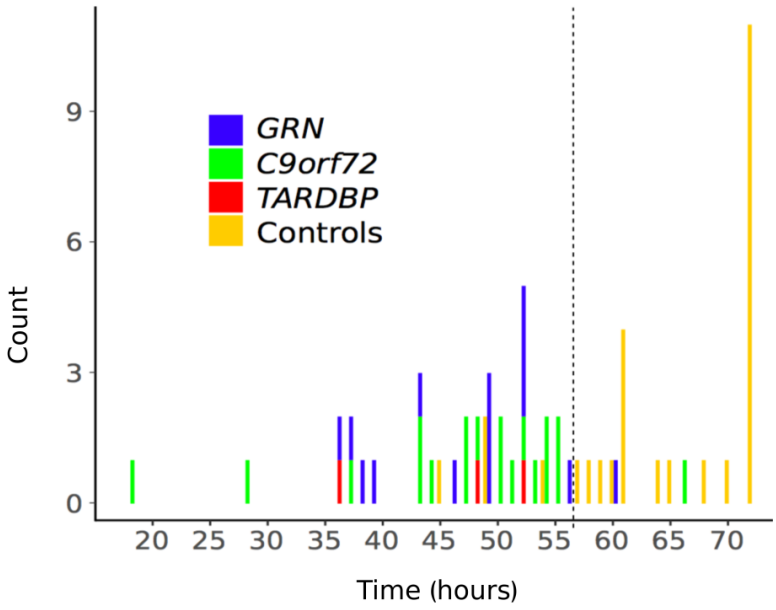

B

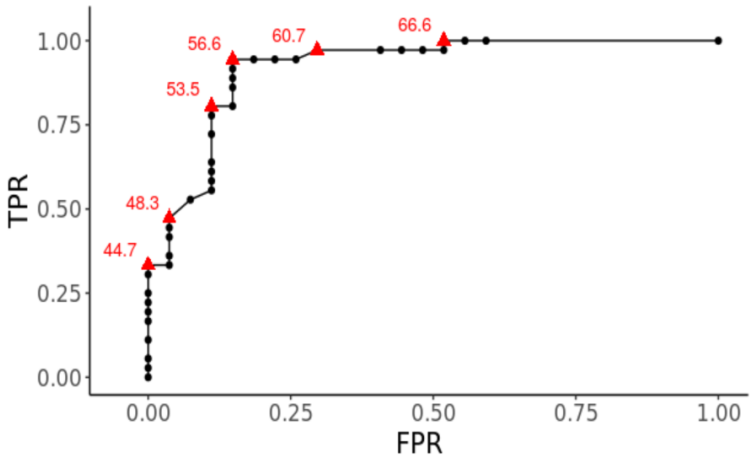

Figure 11: Statistical analysis for lag phase threshold definition. A Distributions of "total median time" values from controls and mutated subjects (see Materials and Methods). The two distributions, even with a certain degree of overlap, differ significantly between each other. Controls: 64.2 ± 8.4 hours, mutated subjects: 46.9 ± 9.1 hours (mean ± standard deviation, SD). The difference is of 17.3 hours with 95% confidence interval (CI) [12.9, 22.8]. A Welch two-sample t-test guarantees the presence of the effect [t (58.4) = 7.8, p = 1.1 10^{-10}]. **B** The ROC (Receiver Operating Characteristic) curve highlights the points with the highest accuracies, illustrating how the choice of the lag phase threshold would influence the True Positive Rate (TPR) and False Positive Rate (FPR) numbers.

CSF samples collected from C9orf72 expansion (n=19), TARDBP (n=3), GRN (n=14) mutation carriers and age-matched controls (n = 27) (see Table 1 for clinical details) were analyzed by means of RT-QuIC to investigate their effects on the kinetics of HuTDP-43(263-414) aggregation. We found that 18 out of 19 *C9orf72*, three out of three *TARDBP* and 13 out of 14 *GRN* samples efficiently seeded the RT-QuIC reaction (Figure 12A, B, C, E). Among age-matched controls, we observed four positive results (Figure 12D, E). These values correspond to a global sensitivity of 94% and specificity of 85%. In order to address the risk of overfitting, we cross-validated our data. The accuracy values predicted by the cross-validation model were 92% and 84% of sensitivity and specificity, respectively, confirming the observed experimental measurements. Among the *GRN* group, notably, one positive sample derived from a healthy carrier of the mutation. There was no significant correlation between baseline characteristics (age at CSF collection, time between disease onset and CSF collection, ALS, FTD, ALS plus FTD or cognitive decline phenotypes) and RT-QuIC positive results. The one *C9orf72* and the one *GRN* negative subjects did not display any difference compared to the other samples, possibly explaining their low seeding efficiency. More in details, they presented clinical features (ALS without cognitive impairment and bv-FTD, respectively), age at CSF collection (45 and 58 years, respectively) and delay from onset to CSF collection (24 months for both patients) comparable to the rest of the patient population (Table 1).

Characteristic	*C9orf72*	*TARDBP*	*GRN*	Totals patients	CTRLs
Men, n. (%)	11 (58)	2 (67)	8 (57)	21 (58)	14 (52)
Age at CSF collection, y. (±SD)	59 ± 10	58 ± 16	63 ± 8	60 ± 10	65 ± 13
Age at onset, y. (±SD)	58 ± 9	55 ± 15	59 ± 4	58 ± 9	N.A.
Onset-CSF collection, m. (±SD)	22 ± 17	32 ± 19	22 ± 9	23 ± 15	N.A.
Pure ALS phenotype, n.	8	3	_	11	N.A.
ALS plus cognitive decline, n.	2	_	_	2	N.A.
Pure FTD, n.	8	_	10	18	N.A.
CBS, n.	_	_	1	1	N.A.
MCI, n.	_	_	1	1	N.A.
AD, n.	1	_	1	2	N.A.
Pre-symptomatic carrier, n.	_	_	1	1	N.A.
Total, n.	19	3	14	36	27
Positive in RT-QuIC, n. (%)	18 (95)	3 (100)	13 (93)	34 (94)	4 (15)

Table 1: Characteristics of CSF study population. Data are presented as numbers (n.), (percentages) and means (±SD). The onset-CSF collection time was calculated in months and refers to the time passed between the onset of disease and the collection of the CSF sample. y.: years; m.: months; CTRLs: age-matched control subjects; N.A.: not applicable. CSF: cerebrospinal fluid; ALS: amyotrophic lateral sclerosis; FTD: frontotemporal dementia; CBS: cortico-basal syndrome; MCI: mild cognitive impairment; AD: Alzheimer disease; RT-QuIC: real time quacking induced convertion.

Regarding the four unexpected positive results among control subjects (i.e. false positive samples), we did not observe any specific feature implicated in their seeding ability. All four subjects were age-matched against the study population and did not present any clinical condition related to neurodegeneration.

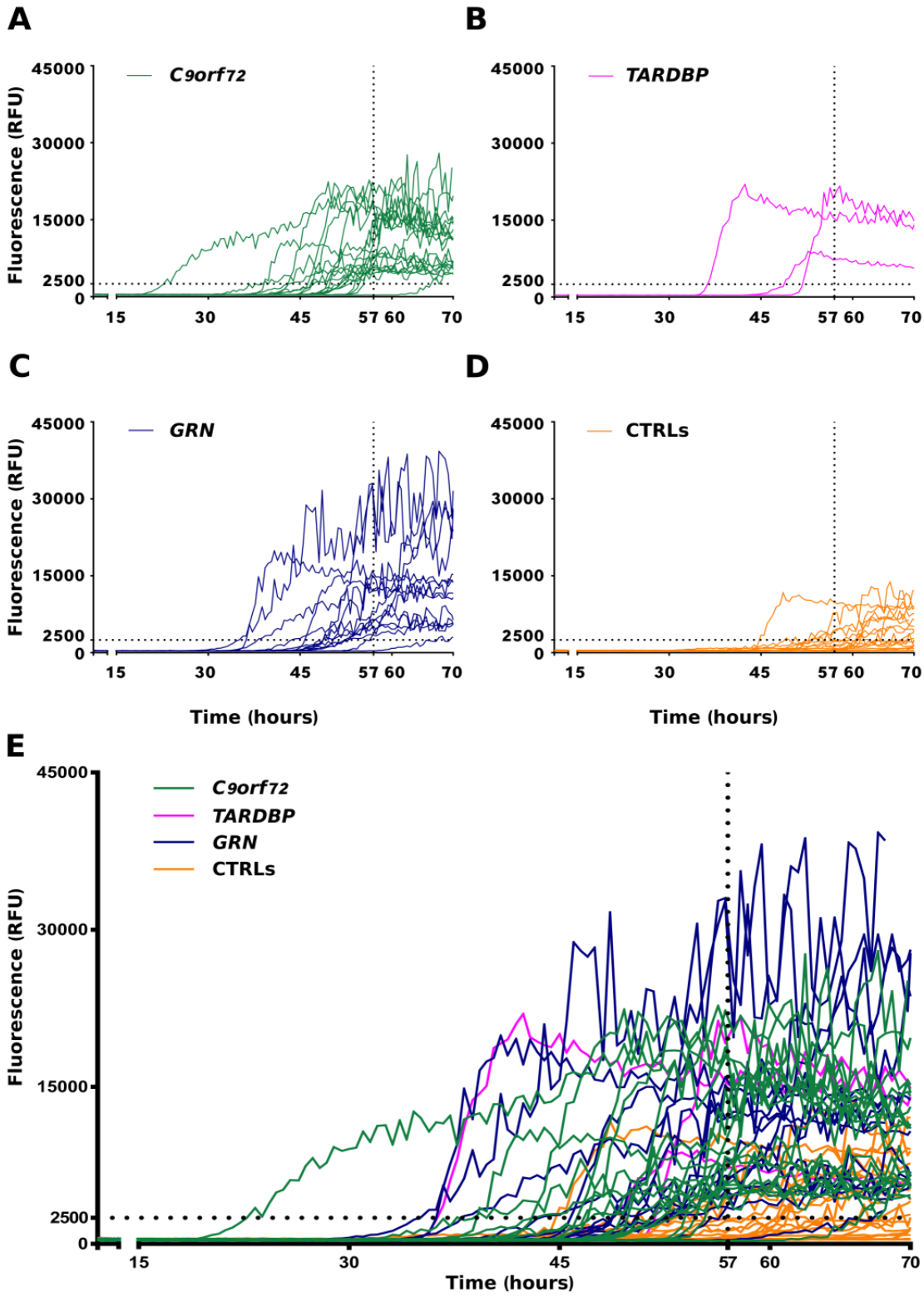

Figure 12: RT-QuIC analysis of ALS and FTLD-TDP CSF samples. 6 µL of undiluted CSF collected from subjects with a known pathological TDP-43 related mutation (*C9orf72*, green lines, *TARDBP*, magenta lines, *GRN*, blue lines) and from age-matched controls (CTRLs, orange lines) were added to purified seed-free recombinant HuTDP-43(263-414) (0.05 mg/mL) and analyzed by means of RT-QuIC with the optimized protocol (shaking at 100 rpm for 15 s every 30 minutes at 40 °C). ThT fluorescence intensity is plotted against time. Dotted black lines represent the ThT fluorescence and lag phase thresholds. In the first four panels (**A, B, C, D**) the curves for each group are displayed separately, while in **E** samples are shown all together. The experiment was performed in triplicate and each replica was performed three times. Each curve displays the median aggregation curve for each sample.

Leukocyte count, glucose, total protein, blood pigments, lactate, and oligoclonal IgG bands were all normal in their CSF. To investigate if the seeding activity of positive CSF samples was driven by the presence of TDP-43 aggregates we used magnetic beads coated with a cocktail composed of two anti-TDP-43 antibodies to immune-deplete one true positive (i.e. a CSF sample from a patient which tested positive in the TDP-43 RT-QuIC assay) and two false positive samples (i.e. samples from two controls which resulted positive in our analysis). After depletion, the true positive sample had an almost abolished seeding activity and tested negative (Figure 13A). This suggests that the procedure was able to deplete it from the majority of TDP-43 aggregates. Regarding the depleted false positive samples, one of them became negative, while the other one remained positive, even if presenting a diminished intensity of ThT fluorescence emission (Figure 13B). This implies that some false positive results may be associated with the presence of TDP-43 aggregates in the CSF of asymptomatic subjects, while some others may be related to the presence/absence of other factors able to interfere with the reaction in a nonspecific way.

4.1.5 Performance of TDP-43 RT-QuIC with tau and α-synuclein aggregates

To investigate the performance of TDP-43 RT-QuIC with aggregates composed of other pathological amyloids, we tested the seeding ability of preformed tau K18 and α-syn fibrils.

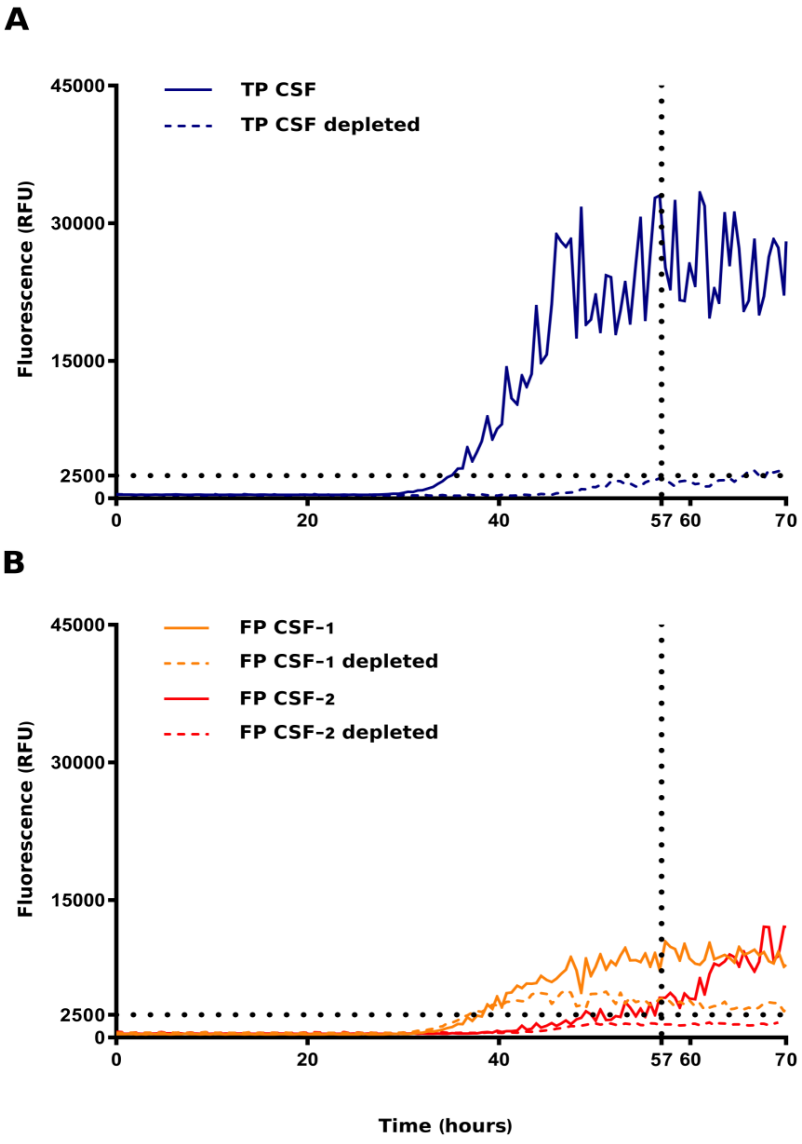

Figure 13: RT-QuIC analysis of immune-depleted CSF samples. One true positive (TP) and two false positive (FP) CSF samples were immune-depleted of TDP-43 aggregates using magnetic beads coated with a cocktail of two anti-TDP-43 antibodies directed against two different epitopes of the protein. Samples before and after immune-depletion were added to purified seed-free recombinant HuTDP-43(263-414) (0.05 mg/mL) and analyzed by means of RT-QuIC (shaking at 100 rpm for 15 s every 30 minutes at 40 °C). ThT fluorescence intensity

is plotted against time. Dotted black lines represent the ThT fluorescence and lag phase thresholds. **A** After depletion the true positive sample tested negative (blue dashed line). **B** After depletion one of the false positive samples became negative (red dashed line), while the other one remained positive, even if presenting a diminished intensity of ThT fluorescence emission (yellow dashed line). The experiment was performed in triplicates and each replica was performed three times. The image represents the median aggregation curve for each sample.

Since we wanted to replicate the same experimental settings that we used for the CSF analysis we diluted tau K18 or α-syn fibrils in a previously screened negative CSF from a control subject. The CSF sample spiked with 1.5 nanograms (ng) of tau K18 or α-syn fibrils presented no seeding activity in the TDP-43 RT-QuIC (Figure 14). Notably, when the same amount of TDP-43 *in vitro* obtained fibrils (1.5 ng) was diluted in the same negative CSF, the sample resulted positive (Figure 14). Tau K18 and α-syn aggregates presented an efficient seeding activity when tested with their respective tau or α-syn RT-QuIC assays. These results suggest that, under these experimental conditions, TDP-43 RT-QuIC is not susceptible to the presence of tau or α-syn amyloids.

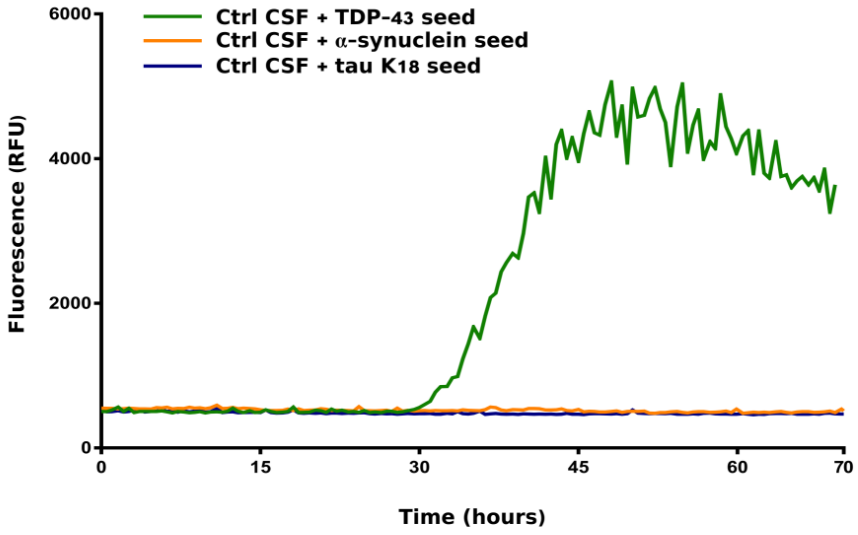

Figure 14: Performance of TDP-43 RT-QuIC with tau and α-synuclein aggregates. A previously screened negative CSF sample was spiked with 1.5 ng of tau K18, α-syn or TDP-43 preformed seeds. CSF samples spiked with tau K18 (blue line) or α-syn (yellow line) fibrils presented no seeding activity in the optimized TDP-43 RT-QuIC. TDP-43 preformed aggregates diluted in the same negative CSF efficiently seeded the reaction (green line). Protocol details: 0.05 mg/mL of purified seed-free recombinant HuTDP-43(263-414) substrate; shaking at 100 rpm for 15 s every 30 minutes at 40 °C. ThT fluorescence intensity is plotted against time. The experiment was performed in triplicates and each replica was performed three times. The image represents the median aggregation curve for each sample.

4.1.6 RT-QuIC detection of aggregated TDP-43

To measure the capabilities of RT-QuIC detection of aggregated TDP-43 we added different dilutions of the *in vitro* obtained HuTDP-43(263-414) aggregates to a previously screened negative CSF sample and tested the seeding activity of these products (Figure 15).

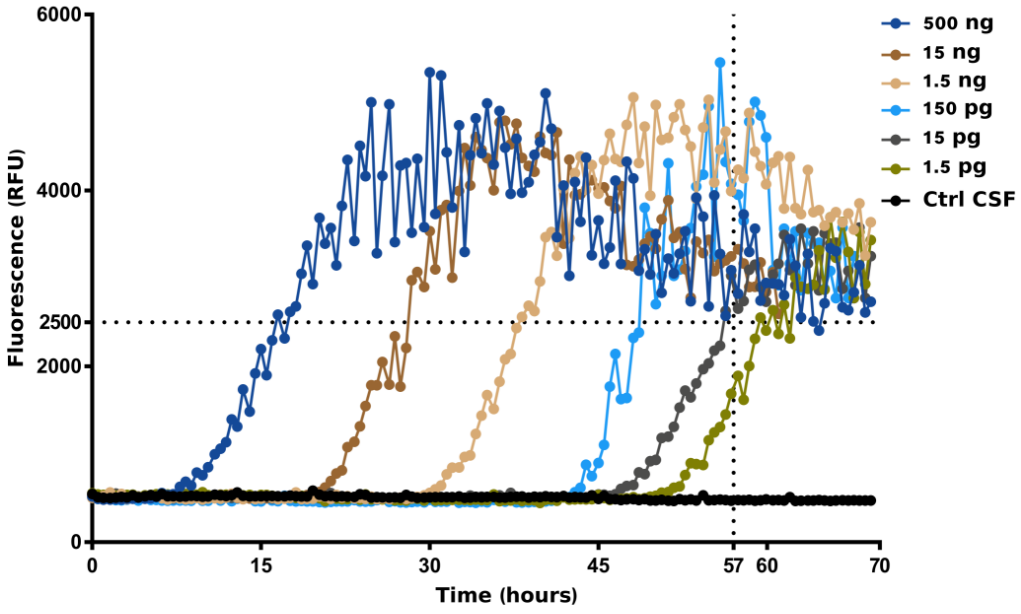

Figure 15: Performance of TDP-43 RT-QuIC with TDP-43 CSF. Different dilutions of *in vitro* obtained HuTDP-43(263-414) aggregates were added to a previously screened negative

CSF sample. TDP-43 RT-QuIC was able to detect as little as 15 pg of TDP-43 pathological aggregates. Protocol details: 0.05 mg/mL of purified seed-free recombinant HuTDP-43(263-414) substrate; shaking at 100 rpm for 15 s every 30 minutes at 40 °C. ThT fluorescence intensity is plotted against time. Dotted black lines represent the ThT fluorescence and lag phase thresholds. The experiment was performed in triplicate and each replica was performed three times. The image represents the median aggregation curve for each sample.

We observed that our assay was able to detect as little as 15 picograms (pg) of TDP-43 pathological aggregates. Since we knew the exact amount of the diluted TDP-43 aggregates, this was the most accurate method in our hands to characterize a dose-response correlation for the optimized RT-QuIC. Furthermore, standard detection techniques failed to quantify the content of pathological hyperphosphorylated TDP-43 in CSF samples from our cohort. For this reason, a dose-response analysis on patient-derived CSF was not feasible. Since our dose-response characterization was performed with the use of synthetic aggregates, which may or may not represent *in vivo* circulating TDP-43 species, further experiments are needed to verify if this estimation also applies to patient-derived samples.

4.2 Part II-uptake and toxicity of synthetic TDP-43 aggregates

4.2.1 TDP-43 fibrils uptake and phosphorylation in SH-SY5Y cells

We exposed SH-SY5Y cells to TDP-43 C-terminal fibrils collected as the final product of *in vitro* aggregation HuTDP-43(263-414), to evaluate their seeding properties. We selected the SH-SY5Y cell line to investigate TDP-43 intra-cellular aggregation since these cells physiologically present adequate basal levels of expression of the endogenous TDP-43 product (Figure 16A). To avoid toxicity due to the presence of ThT or reagents dissolved in the RT-QuIC reaction buffer, fibrils were produced in the absence of ThT and the reaction buffer was

removed by means of ultracentrifugation. HuTDP-43(263-414) fibrils were sonicated, mixed with lipofectamine and added to the cell culture medium to a final concentration of 500 nM. One day after treatment we observed the presence of TDP-43 aggregates within exposed cells (Figure 16B, white arrowheads). Notably, some of the aggregates stained using the C-terminal anti-TDP-43 antibody were also positive for the phospho-specific anti-TDP-43 antibody (Figure 16B, yellow arrowheads). The observation of phosphorylated TDP-43 aggregates suggests that *in vitro* obtained fibrils (intrinsically devoid of post-translational modifications due to the expression in bacteria of the monomeric recombinant protein) were internalized in cells and actively phosphorylated, a feature reminiscent of *in vivo* observed TDP-43 pathology. To further verify that HuTDP-43(263-414) fibrils were internalized within cells, we performed the same experiment with EGFP-over-expressing SH-SY5Y cells, which present a spontaneous fluorescence emission, facilitating the definition of cellular bodies. With this strategy we were able to confirm the internalization HuTDP-43(263-414) fibrils within SH-SY5Y cells (Figure 17A).

4.2.2 TDP-43 fibrils recruit endogenous TDP-43 to form intra-cellular aggregates

TDP-43 aggregates isolated from patient-derived diseased tissues are composed of both the full-length protein and its C-terminal fragments (Nonaka and Hasegawa, 2018). To evaluate the participation of the endogenous full-length TDP-43 in the formation of the observed intra-cellular aggregates, we stained SH-SY5Y cells treated with TDP-43 C-terminal fibrils with an anti-TDP-43 antibody directed against the N-terminus of the protein. Some of the intra-cellular aggregates stained by the phospho-specific anti-TDP-43 antibody were recognized also by the N-terminal specific antibody (Figure 17B), suggesting that the observed positive signal was related to the participation of the endogenous full-length TDP-43. Taken together these

observations suggest that HuTDP-43(263-414) fibrils are internalized into SH-SY5Y cells, actively phosphorylated and that they are able to recruit the endogenous full-length TDP-43 protein to take part in the formation of intra-cellular aggregates.

4.2.3 TDP-43 aggregates are toxic to cells and maintain RNA-binding ability

We observed that cells treated with HuTDP-43(263-414) fibrils at 500 nM concentration presented a severe decrease in their vitality (reduction of ~50%) (Figure 18A).

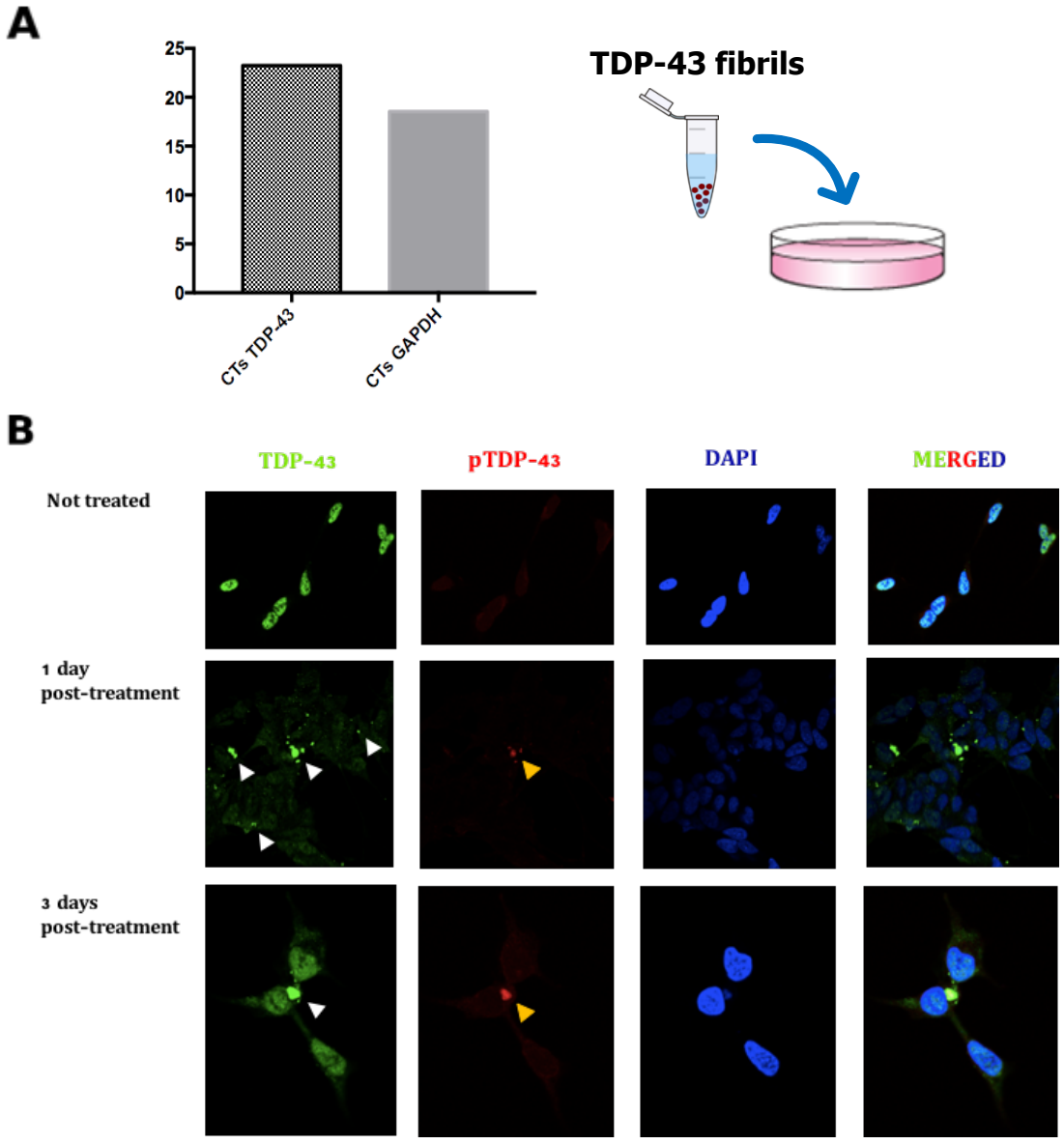

Figure 16: Treatment of SH-SY5Y cells with HuTDP-43(263-414) fibrils. A Real-time quantitative polymerase chain reaction (RT-qPCR) analysis of the expression of endogenous TDP-43 in SH-SY5Y cells compared to the Glyceraldehyde-3-phosphate dehydrogenase (GAPDH) house-keeping gene. CTs: cycle thresholds. The evaluation was performed in triplicate. **B** Cells, at 1- or 3-days post-treatment, present the presence of TDP-43 positive aggregates stained with the rabbit polyclonal anti-TDP-43 C-terminal antibody (white arrowheads). TDP-43 positive aggregates are recognized also by the anti-phospho TDP-43 (Ser409/Ser410) antibody (yellow arrowheads).

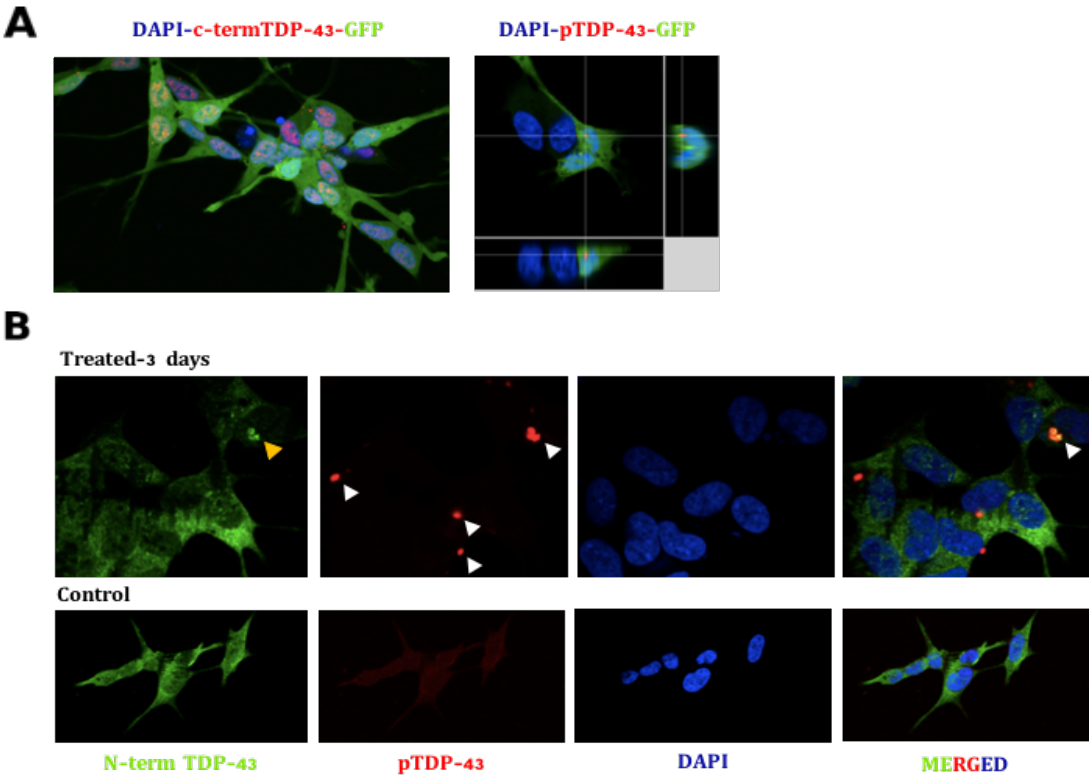

Figure 17: Fluorescence analysis of SH-SY5Y and EGFP-SH-SY5Y cells. A TDP-43 positive aggregates localize within the cytoplasm of EGFP-SH-SY5Y cell, as confirmed by z-stack analysis. **B** pTDP-43 positive aggregates (white arrowheads) induced by the administration of TDP-43 C-terminal fibrils are recognized by the polyclonal N-terminal anti-TDP-43 antibody (yellow arrowhead).

One of the hypothesized mechanisms of toxicity of TDP-43 aggregates within neurons is that TDP-43 accumulation in the cytosol is accompanied by its loss of function in the nuclear compartment, with downstream alterations of several genes under its control (Afroz *et al.*, 2019). To investigate if this was the case in our cellular model, we evaluated TDP-43 function on two among the list of its splicing targets (De Conti *et al.*, 2015), namely the STAG2 and POLDIP3 transcripts and we observed no differences in the representation of their splicing variants between treated and control cells (Figure 18B).

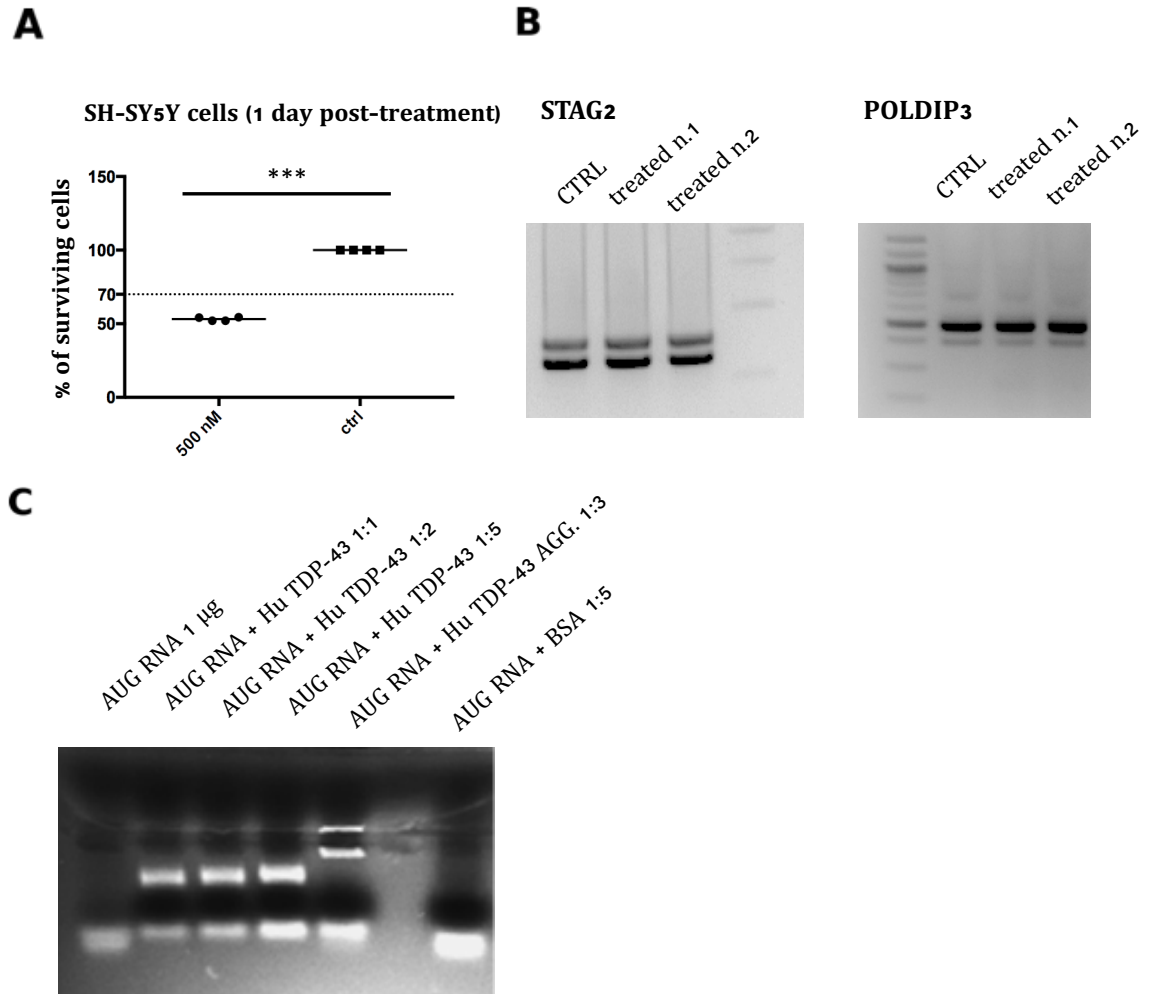

Figure 18: Mechanisms of toxicity of TDP-43 aggregates. A HuTDP-43(263-414) fibrils are toxic when administered to SH-SY5Y cells at 500 nM concentration, as demonstrated by the MTT vitality assay. **B** STAG2 and POLDIP3 genes splicing variant representation is not modified in SH-SY5Y cells upon treatment with HuTDP-43(263-414) fibrils. **C** shows the

results of the EMSA: The first line corresponds to free AUG12 RNA (12.5 μM), line 2,3 and 4 to the same amount of AUG12 RNA mixed with increasing concentrations of the monomeric HuTDP-43 at a 1:1, 1:2 and 1:5 molar ratios, respectively. Line 5 corresponds to AUG12 RNA (12.5 μM) mixed with HuTDP-43 aggregates obtained *in vitro* at 1:3 molar ratio. The last line refers to AUG12 RNA mixed with Bovine Serum Albumin (BSA) at 1:5 same molar ratio, as a control. The specific banding shift observed in the presence of HuTDP-43 aggregates suggests that they maintain the RNA-binding property.

Another suggested mechanism of toxicity for intra-cellular TDP-43 aggregates is that they can sequester circulating cytoplasmatic RNA molecules, disrupting normal RNA metabolism and/or trafficking. To investigate if full-length TDP-43 aggregates maintain the RNA-binding ability typical of the monomeric protein we isolated *in vitro* obtained full-length HuTDP-43 aggregates and performed the EMSA using again the AUG12 RNA as the RNA probe. Only when AUG12 RNA was exposed to full-length HuTDP-43 aggregates we observed a specific shift in the RNA migration banding pattern, characterized by the presence of RNA molecules "trapped" within the well of the agarose gel (Figure 18C, fifth line). This pattern was specifically related to the interaction between AUG12 RNA and HuTDP-43 aggregates, since it was not observed when the RNA probe was exposed to increasing concentrations of the monomeric protein (Figure 18C line 2, 3, 4). Since our analysis was performed with *in vitro* obtained aggregates, which may or may not represent intra-cellular and/or *in vivo* circulating TDP-43 species, further experiments are needed to verify these results.

CHAPTER V

5. DISCUSSION

5.1 Development and optimization of the TDP-43 RT-QuIC

Despite many efforts, ALS and FTD still lack treatments able to interfere with the underlying pathological process. One reason is the absence of an early diagnostic biomarker able to detect the disease before irreversible neuronal damage has occurred. In fact, like amyloid beta deposition in AD (Bateman *et al.*, 2012), it is possible that also the formation and accumulation of pathological aggregates of misfolded TDP-43 species could begin decades before symptoms onset. As a consequence, patients are usually enrolled in trials in advanced clinical phases when neuronal damage and the neurodegenerative process have already started, thus decreasing the potential efficacy of tested compounds. The availability of a reliable biochemical marker could also help in monitoring disease progression in the evaluation of response to a specific treatment. Our approach to detect the presence of pathological TDP-43 species in the CSF of ALS and FTD patients was to exploit the RT-QuIC intrinsic ability to amplify minutes amount of misfolded proteins. Since this technology proved to efficiently perform with prions and several other prion-like proteins (Orru *et al.*, 2014; Salvadores *et al.*, 2014; Orru *et al.*, 2015; Fairfoul *et al.*, 2016; Franceschini *et al.*, 2017; Saijo *et al.*, 2017; Shahnawaz *et al.*, 2017; Groveman *et al.*, 2018; van Rumund *et al.*, 2019) and since TDP-43 displayed prion-like features, we aimed at optimizing it for TDP-43. We report that recombinant human TDP-43 is a suitable substrate to perform the RT-QuIC reaction. We describe an efficient protocol for a large-scale production and purification of both full-length and truncated TDP-43, essential to set up and perform the RT-QuIC technique. As a first step in TDP-43 RT-QuIC adaptation, we used the final products

of aggregation of both HuTDP-43 and HuTDP-43(263-414) proteins which efficiently seeded the reaction and we subsequently moved to the study of a small subset of brain homogenates derived from autopsy-verified TDP-43 positive cases. We selected TDP-43 C-terminal fragment as the best substrate for a large-scale sample screening. We collected CSF samples from subjects harboring a pathological mutation in one of the genes known to cause TDP-43 deposition in the CNS. This approach implied at least two advantages: i) even without a neuropathological confirmation, the presence of a known pathological TDP-43-related mutation increased the likelihood that those CSF contained toxic TDP-43 species ii) analyzing CSF from patients with a TDP-43 related mutation reduced the pathological uncertainty related to heterogeneous clinical presentations. This second observation explains our decision to collect CSF also from subjects with a clinical diagnosis different than classical ALS and FTD, as long as they harbored a TDP-43-related pathological mutation. Our data suggest that TDP-43 RT-QuIC is able to discriminate between a cohort of subjects affected by ALS and FTD and age-matched controls with a total sensitivity of 94% and a specificity of 85%, detecting as little as 15 picograms of TDP-43 seed. Among the *GRN* group we also tested one pre-symptomatic carrier that resulted positive. This subject to date is still asymptomatic and is under clinical follow-up. Since the co-deposition of TDP-43 and other pathological proteins occurs frequently in many neurodegenerative disorders (Amador-Ortiz *et al.*, 2007; Freeman *et al.*, 2008; Lin and Dickson, 2008; Arai *et al.*, 2009; Josephs *et al.*, 2016; Berning and Walker, 2019), we considered inaccurate to use CSF samples derived from patients affected by other neurodegenerative diseases to assess the presence of cross-seeding. To overcome this potential limitation and to maintain the experimental settings of the CSF-optimized RT-QuIC technology, we diluted 1.5 ng of tau K18 and α-syn preformed aggregates in a negative CSF sample and we observed no cross-seeding activity. Our study is not without limitations. First, sensitivity and specificity of our protocol are lower than desired. According to the analysis on

depleted false positive samples, it seems that false positivity could be related to multiple factors. The fact that one false positive sample became negative after the TDP-43 depletion protocol, suggests that at least some of the observed false positive results could be due to the presence of TDP-43 aggregates in the CSF of asymptomatic subjects. Since we do not possess neuropathological confirmation for the examined samples, it is not possible to exclude that we have detected the presence of pathological TDP-43 seeds in healthy subjects that would eventually develop a TDP-43 related disorder during their life span. In this regard, it should be mentioned that several reports observed the presence of age-dependent TDP-43 deposition in a discrete proportion of cognitively impaired but also healthy subjects (Geser *et al.*, 2010; Uchino *et al.*, 2015). The fact that one false positive sample remained positive also after depletion, suggests that some of the observed false positive results might be intrinsically related to CSF composition. CSF samples, in fact, may differ for the presence or absence of specific molecules able to modify the kinetics of aggregation of the substrate in a nonspecific way, independent of the presence of aggregates. A preparation method able to remove, or at least limit, possible TDP-43 interactors in the analyzed samples needs to be implemented to overcome this potential limitation. We would also like to test other patient-derived tissues, to evaluate their characteristics and seeding efficiency. A second limitation of our study is the number of tested subjects. On one hand the decision to focus on a selected population of patients (i.e. the ones with a known TDP-43-related pathogenic mutation) increased the likelihood that the suspected positive CSF really contained TDP-43 seeds. On the other hand, since these mutations are quite rare, it reduced our sample size. Even with this limitation, we considered this approach as the most efficient in the adaptation of this technology to TDP-43.

5.2 Uptake and toxicity of synthetic TDP-43 aggregates

TDP-43 proteinopathies are characterized by the pathological accumulation of TDP-43 aggregates within the cytoplasm of neuronal and glial cells accompanied by the loss of the nuclear protein (Nonaka and Hasegawa, 2018). We performed a preliminary evaluation of the seeding properties of *in vitro* obtained TDP-43 synthetic aggregates in a cellular model, in order to evaluate their ability to recapitulate ALS/FTD TDP-43 pathology. For this purpose, we exposed SH-SY5Y cells to the *in vitro* generated TDP-43 C-terminal (HuTDP-43(263-414)) fibrils and observed their fate and toxicity. We selected the SH-SY5Y cell line to investigate TDP-43 intra-cellular aggregation since they physiologically express adequate levels of the endogenous TDP-43 product. We observed that HuTDP-43(263-414) fibrils are readily internalized and actively phosphorylated in SH-SY5Y cells. Furthermore, TDP-43 aggregates were not composed only of the C-terminal portion of the protein but were positively stained with an antibody which selectively recognizes the TDP-43 N-terminal domain. This suggest that TDP-43 C-terminal fibrils are able to recruit the full-length endogenous protein in the formation of intra-cellular aggregates composed of hyperphosphorylated forms of the protein. Next, we evaluated the effect of the formation of TDP-43 aggregates in SH-SY5Y cells, observing that they resulted in a severe reduction of cell vitality (~50%). This observed toxicity was not associated with a TDP-43 nuclear loss of function. Our preliminary results, conducted with synthetic recombinant full-length TDP-43 aggregates, suggest that the observed detrimental effects could be due to a disruption of normal RNA trafficking/metabolism. In fact, we observed that amorphous aggregates obtained with our *in vitro* assay and composed of the full-length protein, maintain the RNA-binding ability characteristic of the monomeric protein, suggesting the intriguing possibility that TDP-43 aggregates sequester circulating RNA molecules, with detrimental downstream effects. Since our analysis was performed with *in vitro* obtained aggregates, which may or may not represent intra-cellular and/or *in vivo* circulating TDP-43 species, further experiments are needed to verify our hypothesis.

5.3 Conclusions

We described a robust protocol for large-scale production of recombinant TDP-43 and for its use as a substrate in the RT-QuIC reaction. Furthermore, we analyzed the kinetics of aggregation of both full-length and C-terminal (263-414) human TDP-43, showing that their features are intrinsically related to the structure acquired during aggregation. We adapted the RT-QuIC technology with both substrates and we selected HuTDP-43(263-414) as the best candidate to perform a large population screening. We modified the protocol settings for the reaction with the HuTDP-43(263-414) substrate in order to decrease the time-course of its kinetics of aggregation and to dispose of the largest lag phase time-window. After this optimization we collected and screened the CSF of ALS and FTD subjects harboring a pathological mutation in the *GRN*, *TARDBP* or *C9orf72* genes and age-matched controls. The TDP-43 RT-QuIC was able to detect as little as 15 pg of TDP-43 aggregates reaching a total sensitivity of 94% and a specificity of 85%. Furthermore, heterologous seeds of tau K18 and α-syn preformed aggregates presented no signs of cross-seeding interaction with the substrate. Finally, immune-depletion analysis on false positive samples suggested that some false positive result may be related to the detection of TDP-43 circulating aggregates in the CSF of healthy subjects (which may develop or not a TDP-43-related disorder), but also to the heterogeneity of the CSF material.

We performed a preliminary evaluation of the seeding properties of the *in vitro* obtained TDP-43 synthetic aggregates in a cellular model, in order to evaluate their ability to recapitulate ALS/FTD TDP-43 pathology. For this purpose, we treated SH-SY5Y cells with *in vitro* generated TDP-43 C-terminal fibrils and observed that they were readily internalized and actively phosphorylated. Furthermore, TDP-43 C-terminal fibrils were able to recruit the full-length endogenous protein in the formation of intra-cellular aggregates composed of

hyperphosphorylated forms of the protein. All these features are reminiscent of TDP-43 *in vivo* pathology. The formation of TDP-43 intra-cellular aggregates resulted in a severe reduction of cell vitality which was not linked to a TDP-43 loss of function. We hypothesized that the observed detrimental effects could be related to a maintained RNA-binding capacity of TDP-43 aggregates and provided preliminary evidence supporting this hypothesis.

In conclusion, our data represent a proof-of-concept of TDP-43 RT-QuIC potential for the detection of TDP-43 pathological aggregates. Together with prion, amyloid beta, tau and α-syn RT-QuIC assays, a further optimization of the presented TDP-43 RT-QuIC protocol, would increase the opportunity to perform the earliest and most accurate diagnosis at a single patient level. Furthermore, we showed that CSF detection of TDP-43 pathological aggregates may be exploited as a disease biomarker for ALS and FTD. Our preliminary results regarding the seeding properties of TDP-43 synthetic aggregates suggest that TDP-43 RT-QuIC could be exploited not only as a powerful drug screening and diagnostic tool but could also serve as a very helpful instrument to further elucidate TDP-43 prion-like features.

APPENDIX

SUPPLEMENTARY MATERIALS

Patient code	Pathological Mutation	Positive in RT-QuIC (Y/N)
*C9orf72*_1	C9orf72 expansion	Y
*C9orf72*_2	C9orf72 expansion	Y
*C9orf72*_3	C9orf72 expansion	Y
*C9orf72*_4	C9orf72 expansion	Y
*C9orf72*_5	C9orf72 expansion	N
*C9orf72*_6	C9orf72 expansion	Y
*C9orf72*_7	C9orf72 expansion	Y
*C9orf72*_8	C9orf72 expansion	Y
*C9orf72*_9	C9orf72 expansion	Y
*C9orf72*_10	C9orf72 expansion	Y
*C9orf72*_11	C9orf72 expansion	Y
*C9orf72*_12	C9orf72 expansion	Y
*C9orf72*_13	C9orf72 expansion	Y
*C9orf72*_14	C9orf72 expansion	Y
*C9orf72*_15	C9orf72 expansion	Y
*C9orf72*_16	C9orf72 expansion	Y
*C9orf72*_17	C9orf72 expansion	Y
*C9orf72*_18	C9orf72 expansion	Y
*C9orf72*_19	C9orf72 expansion	Y
*TARDBP*_1	p.Ser387delinsThrAsnPro	Y
*TARDBP*_2	p.Ser387delinsThrAsnPro	Y
*TARDBP*_3	p.Ala382Thr	Y
*GRN*_1	p.Leu271LeufsX10	Y
*GRN*_2	p.Leu271LeufsX10	Y
*GRN*_3	p.Leu271LeufsX10	Y
*GRN*_4	p.Leu271LeufsX10	Y

***GRN*_5**	**p.Leu271LeufsX10**	**Y**
***GRN*_6**	**p.Leu271LeufsX10**	**Y**
***GRN*_7**	**p.Leu271LeufsX10**	**N**
***GRN*_8**	**p.Leu271LeufsX10**	**Y**
***GRN*_9**	**p.Leu271LeufsX10**	**Y**
***GRN*_10**	**p.Leu271LeufsX10**	**Y**
***GRN*_11**	**p.Thr276SerfsX7**	**Y**
***GRN*_12**	**p.Leu271LeufsX10**	**Y**
***GRN*_13**	**p.Leu271LeufsX10**	**Y**
***GRN*_14**	**p.Leu271LeufsX10**	**Y**

Supplementary Table 1: List of pathological genetic mutations in the study cohort.

REFERENCES

Afroz, T., E. M. Hock, P. Ernst, C. Foglieni, M. Jambeau, L. A. B. Gilhespy*, et al.* (2017). "Functional and dynamic polymerization of the ALS-linked protein TDP-43 antagonizes its pathologic aggregation." Nat Commun **8**(1): 45.

Afroz, T., M. Perez-Berlanga and M. Polymenidou (2019). "Structural Transition, Function and Dysfunction of TDP-43 in Neurodegenerative Diseases." Chimia (Aarau) **73**(6): 380-390.

Aguzzi, A. (2009). "Cell biology: Beyond the prion principle." Nature **459**(7249): 924-925.

Alami, N. H., R. B. Smith, M. A. Carrasco, L. A. Williams, C. S. Winborn, S. S. W. Han*, et al.* (2014). "Axonal transport of TDP-43 mRNA granules is impaired by ALS-causing mutations." Neuron **81**(3): 536-543.

Amador-Ortiz, C., W. L. Lin, Z. Ahmed, D. Personett, P. Davies, R. Duara*, et al.* (2007). "TDP-43 immunoreactivity in hippocampal sclerosis and Alzheimer's disease." Ann Neurol **61**(5): 435-445.

Arai, T., M. Hasegawa, H. Akiyama, K. Ikeda, T. Nonaka, H. Mori*, et al.* (2006). "TDP-43 is a component of ubiquitin-positive tau-negative inclusions in frontotemporal lobar degeneration and amyotrophic lateral sclerosis." Biochem Biophys Res Commun **351**(3): 602-611.

Arai, T., I. R. Mackenzie, M. Hasegawa, T. Nonoka, K. Niizato, K. Tsuchiya*, et al.* (2009). "Phosphorylated TDP-43 in Alzheimer's disease and dementia with Lewy bodies." Acta Neuropathol **117**(2): 125-136.

Armstrong, M. J., I. Litvan, A. E. Lang, T. H. Bak, K. P. Bhatia, B. Borroni*, et al.* (2013). "Criteria for the diagnosis of corticobasal degeneration." Neurology **80**(5): 496-503.

Atarashi, R., J. M. Wilham, L. Christensen, A. G. Hughson, R. A. Moore, L. M. Johnson*, et al.* (2008). "Simplified ultrasensitive prion detection by recombinant PrP conversion with shaking." Nat Methods **5**(3): 211-212.

Avendano-Vazquez, S. E., A. Dhir, S. Bembich, E. Buratti, N. Proudfoot and F. E. Baralle (2012). "Autoregulation of TDP-43 mRNA levels involves interplay between transcription, splicing, and alternative polyA site selection." Genes Dev **26**(15): 1679-1684.

Ayala, Y. M., L. De Conti, S. E. Avendano-Vazquez, A. Dhir, M. Romano, A. D'Ambrogio*, et al.* (2011). "TDP-43 regulates its mRNA levels through a negative feedback loop." EMBO J **30**(2): 277-288.

Ayala, Y. M., S. Pantano, A. D'Ambrogio, E. Buratti, A. Brindisi, C. Marchetti*, et al.* (2005). "Human, Drosophila, and C.elegans TDP43: nucleic acid binding properties and splicing regulatory function." J Mol Biol **348**(3): 575-588.

Baker, M., I. R. Mackenzie, S. M. Pickering-Brown, J. Gass, R. Rademakers, C. Lindholm*, et al.* (2006). "Mutations in progranulin cause tau-negative frontotemporal dementia linked to chromosome 17." Nature **442**(7105): 916-919.

Barghorn, S., J. Biernat and E. Mandelkow (2005). "Purification of recombinant tau protein and preparation of Alzheimer-paired helical filaments in vitro." Methods Mol Biol **299**: 35-51.

Bartz, J. C., R. A. Bessen, D. McKenzie, R. F. Marsh and J. M. Aiken (2000). "Adaptation and selection of prion protein strain conformations following interspecies transmission of transmissible mink encephalopathy." J Virol **74**(12): 5542-5547.

Bateman, R. J., C. Xiong, T. L. Benzinger, A. M. Fagan, A. Goate, N. C. Fox*, et al.* (2012). "Clinical and biomarker changes in dominantly inherited Alzheimer's disease." N Engl J Med **367**(9): 795-804.

Berning, B. A. and A. K. Walker (2019). "The Pathobiology of TDP-43 C-Terminal Fragments in ALS and FTLD." Front Neurosci **13**: 335.

Bigio, E. H., J. Y. Wu, H. X. Deng, E. N. Bit-Ivan, Q. Mao, R. Ganti*, et al.* (2013). "Inclusions in frontotemporal lobar degeneration with TDP-43 proteinopathy (FTLD-TDP) and

amyotrophic lateral sclerosis (ALS), but not FTLD with FUS proteinopathy (FTLD-FUS), have properties of amyloid." Acta Neuropathol **125**(3): 463-465.

Bistaffa, E., F. Moda, T. Virgilio, I. Campagnani, C. M. G. De Luca, M. Rossi*, et al.* (2018). "Synthetic Prion Selection and Adaptation." Mol Neurobiol.

Bongianni, M., C. Orru, B. R. Groveman, L. Sacchetto, M. Fiorini, G. Tonoli*, et al.* (2017). "Diagnosis of Human Prion Disease Using Real-Time Quaking-Induced Conversion Testing of Olfactory Mucosa and Cerebrospinal Fluid Samples." JAMA Neurol **74**(2): 155-162.

Brooks, B. R., R. G. Miller, M. Swash, T. L. Munsat and D. World Federation of Neurology Research Group on Motor Neuron (2000). "El Escorial revisited: revised criteria for the diagnosis of amyotrophic lateral sclerosis." Amyotroph Lateral Scler Other Motor Neuron Disord **1**(5): 293-299.

Budini, M., E. Buratti, C. Stuani, C. Guarnaccia, V. Romano, L. De Conti*, et al.* (2012). "Cellular model of TAR DNA-binding protein 43 (TDP-43) aggregation based on its C-terminal Gln/Asn-rich region." J Biol Chem **287**(10): 7512-7525.

Buratti, E., A. Brindisi, M. Giombi, S. Tisminetzky, Y. M. Ayala and F. E. Baralle (2005). "TDP-43 binds heterogeneous nuclear ribonucleoprotein A/B through its C-terminal tail: an important region for the inhibition of cystic fibrosis transmembrane conductance regulator exon 9 splicing." J Biol Chem **280**(45): 37572-37584.

Buratti, E., T. Dork, E. Zuccato, F. Pagani, M. Romano and F. E. Baralle (2001). "Nuclear factor TDP-43 and SR proteins promote in vitro and in vivo CFTR exon 9 skipping." EMBO J **20**(7): 1774-1784.

Candelise, N., S. Baiardi, A. Franceschini, M. Rossi and P. Parchi (2020). "Towards an improved early diagnosis of neurodegenerative diseases: the emerging role of in vitro conversion assays for protein amyloids." Acta Neuropathol Commun **8**(1): 117.

Casafont, I., R. Bengoechea, O. Tapia, M. T. Berciano and M. Lafarga (2009). "TDP-43 localizes in mRNA transcription and processing sites in mammalian neurons." J Struct Biol **167**(3): 235-241.

Colby, D. W., K. Giles, G. Legname, H. Wille, I. V. Baskakov, S. J. DeArmond*, et al.* (2009). "Design and construction of diverse mammalian prion strains." Proc Natl Acad Sci U S A **106**(48): 20417-20422.

Colby, D. W., Q. Zhang, S. Wang, D. Groth, G. Legname, D. Riesner*, et al.* (2007). "Prion detection by an amyloid seeding assay." Proc Natl Acad Sci U S A **104**(52): 20914-20919.

Condello, C., T. Lemmin, J. Stohr, M. Nick, Y. Wu, A. M. Maxwell*, et al.* (2018). "Structural heterogeneity and intersubject variability of Abeta in familial and sporadic Alzheimer's disease." Proc Natl Acad Sci U S A **115**(4): E782-E791.

Conicella, A. E., G. H. Zerze, J. Mittal and N. L. Fawzi (2016). "ALS Mutations Disrupt Phase Separation Mediated by alpha-Helical Structure in the TDP-43 Low-Complexity C-Terminal Domain." Structure **24**(9): 1537-1549.

Cruts, M., S. Kumar-Singh and C. Van Broeckhoven (2006). "Progranulin mutations in ubiquitin-positive frontotemporal dementia linked to chromosome 17q21." Curr Alzheimer Res **3**(5): 485-491.

D'Alton, S., M. Altshuler and J. Lewis (2015). "Studies of alternative isoforms provide insight into TDP-43 autoregulation and pathogenesis." RNA **21**(8): 1419-1432.

De Conti, L., M. V. Akinyi, R. Mendoza-Maldonado, M. Romano, M. Baralle and E. Buratti (2015). "TDP-43 affects splicing profiles and isoform production of genes involved in the apoptotic and mitotic cellular pathways." Nucleic Acids Res **43**(18): 8990-9005.

DeJesus-Hernandez, M., I. R. Mackenzie, B. F. Boeve, A. L. Boxer, M. Baker, N. J. Rutherford*, et al.* (2011). "Expanded GGGGCC hexanucleotide repeat in noncoding region of C9ORF72 causes chromosome 9p-linked FTD and ALS." Neuron **72**(2): 245-256.

Deng, H. X., W. Chen, S. T. Hong, K. M. Boycott, G. H. Gorrie, N. Siddique*, et al.* (2011). "Mutations in UBQLN2 cause dominant X-linked juvenile and adult-onset ALS and ALS/dementia." Nature **477**(7363): 211-215.

Dewey, C. M., B. Cenik, C. F. Sephton, D. R. Dries, P. Mayer, 3rd, S. K. Good*, et al.* (2011). "TDP-43 is directed to stress granules by sorbitol, a novel physiological osmotic and oxidative stressor." Mol Cell Biol **31**(5): 1098-1108.

Di Fede, G., M. Catania, E. Maderna, R. Ghidoni, L. Benussi, E. Tonoli*, et al.* (2018). "Molecular subtypes of Alzheimer's disease." Sci Rep **8**(1): 3269.

Ederle, H., C. Funk, C. Abou-Ajram, S. Hutten, E. B. E. Funk, R. H. Kehlenbach*, et al.* (2018). "Nuclear egress of TDP-43 and FUS occurs independently of Exportin-1/CRM1." Sci Rep **8**(1): 7084.

Fairfoul, G., L. I. McGuire, S. Pal, J. W. Ironside, J. Neumann, S. Christie*, et al.* (2016). "Alpha-synuclein RT-QuIC in the CSF of patients with alpha-synucleinopathies." Ann Clin Transl Neurol **3**(10): 812-818.

Feneberg, E., E. Gray, O. Ansorge, K. Talbot and M. R. Turner (2018). "Towards a TDP-43-Based Biomarker for ALS and FTLD." Mol Neurobiol **55**(10): 7789-7801.

Franceschini, A., S. Baiardi, A. G. Hughson, N. McKenzie, F. Moda, M. Rossi*, et al.* (2017). "High diagnostic value of second generation CSF RT-QuIC across the wide spectrum of CJD prions." Sci Rep **7**(1): 10655.

Francois-Moutal, L., S. Perez-Miller, D. D. Scott, V. G. Miranda, N. Mollasalehi and M. Khanna (2019). "Structural Insights Into TDP-43 and Effects of Post-translational Modifications." Front Mol Neurosci **12**: 301.

Freeman, S. H., T. Spires-Jones, B. T. Hyman, J. H. Growdon and M. P. Frosch (2008). "TAR-DNA binding protein 43 in Pick disease." J Neuropathol Exp Neurol **67**(1): 62-67.

Freibaum, B. D., R. K. Chitta, A. A. High and J. P. Taylor (2010). "Global analysis of TDP-43 interacting proteins reveals strong association with RNA splicing and translation machinery." J Proteome Res **9**(2): 1104-1120.

Furukawa, Y., K. Kaneko, S. Watanabe, K. Yamanaka and N. Nukina (2011). "A seeding reaction recapitulates intracellular formation of Sarkosyl-insoluble transactivation response element (TAR) DNA-binding protein-43 inclusions." J Biol Chem **286**(21): 18664-18672.

Gasset-Rosa, F., S. Lu, H. Yu, C. Chen, Z. Melamed, L. Guo*, et al.* (2019). "Cytoplasmic TDP-43 De-mixing Independent of Stress Granules Drives Inhibition of Nuclear Import, Loss of Nuclear TDP-43, and Cell Death." Neuron **102**(2): 339-357 e337.

Geser, F., M. Martinez-Lage, J. Robinson, K. Uryu, M. Neumann, N. J. Brandmeir*, et al.* (2009). "Clinical and pathological continuum of multisystem TDP-43 proteinopathies." Arch Neurol **66**(2): 180-189.

Geser, F., J. L. Robinson, J. A. Malunda, S. X. Xie, C. M. Clark, L. K. Kwong*, et al.* (2010). "Pathological 43-kDa transactivation response DNA-binding protein in older adults with and without severe mental illness." Arch Neurol **67**(10): 1238-1250.

Gorno-Tempini, M. L., A. E. Hillis, S. Weintraub, A. Kertesz, M. Mendez, S. F. Cappa*, et al.* (2011). "Classification of primary progressive aphasia and its variants." Neurology **76**(11): 1006-1014.

Groveman, B. R., C. D. Orru, A. G. Hughson, L. D. Raymond, G. Zanusso, B. Ghetti*, et al.* (2018). "Rapid and ultra-sensitive quantitation of disease-associated alpha-synuclein seeds in brain and cerebrospinal fluid by alphaSyn RT-QuIC." Acta Neuropathol Commun **6**(1): 7.

Guenther, E. L., Q. Cao, H. Trinh, J. Lu, M. R. Sawaya, D. Cascio*, et al.* (2018). "Atomic structures of TDP-43 LCD segments and insights into reversible or pathogenic aggregation." Nat Struct Mol Biol **25**(6): 463-471.

Han, T. W., M. Kato, S. Xie, L. C. Wu, H. Mirzaei, J. Pei*, et al.* (2012). "Cell-free formation of RNA granules: bound RNAs identify features and components of cellular assemblies." Cell **149**(4): 768-779.

Hasegawa, M., T. Arai, H. Akiyama, T. Nonaka, H. Mori, T. Hashimoto*, et al.* (2007). "TDP-43 is deposited in the Guam parkinsonism-dementia complex brains." Brain **130**(Pt 5): 1386-1394.

Hasegawa, M., T. Arai, T. Nonaka, F. Kametani, M. Yoshida, Y. Hashizume*, et al.* (2008). "Phosphorylated TDP-43 in frontotemporal lobar degeneration and amyotrophic lateral sclerosis." Ann Neurol **64**(1): 60-70.

Hodges, J. R. and B. Miller (2001). "The classification, genetics and neuropathology of frontotemporal dementia. Introduction to the special topic papers: Part I." Neurocase **7**(1): 31-35.

Holmes, B. B. and M. I. Diamond (2012). "Amyotrophic lateral sclerosis and organ donation: is there risk of disease transmission?" Ann Neurol **72**(6): 832-836.

Huang, C., G. Ren, H. Zhou and C. C. Wang (2005). "A new method for purification of recombinant human alpha-synuclein in Escherichia coli." Protein Expr Purif **42**(1): 173-177.

Hutton, M., C. L. Lendon, P. Rizzu, M. Baker, S. Froelich, H. Houlden*, et al.* (1998). "Association of missense and 5'-splice-site mutations in tau with the inherited dementia FTDP-17." Nature **393**(6686): 702-705.

Inukai, Y., T. Nonaka, T. Arai, M. Yoshida, Y. Hashizume, T. G. Beach*, et al.* (2008). "Abnormal phosphorylation of Ser409/410 of TDP-43 in FTLD-U and ALS." FEBS Lett **582**(19): 2899-2904.

Irwin, D. J., N. J. Cairns, M. Grossman, C. T. McMillan, E. B. Lee, V. M. Van Deerlin*, et al.* (2015). "Frontotemporal lobar degeneration: defining phenotypic diversity through personalized medicine." Acta Neuropathol **129**(4): 469-491.

Ishiguro, A., N. Kimura, Y. Watanabe, S. Watanabe and A. Ishihama (2016). "TDP-43 binds and transports G-quadruplex-containing mRNAs into neurites for local translation." Genes Cells **21**(5): 466-481.

Jiang, L. L., M. X. Che, J. Zhao, C. J. Zhou, M. Y. Xie, H. Y. Li*, et al.* (2013). "Structural transformation of the amyloidogenic core region of TDP-43 protein initiates its aggregation and cytoplasmic inclusion." J Biol Chem **288**(27): 19614-19624.

Johnson, B. S., D. Snead, J. J. Lee, J. M. McCaffery, J. Shorter and A. D. Gitler (2009). "TDP-43 is intrinsically aggregation-prone, and amyotrophic lateral sclerosis-linked mutations accelerate aggregation and increase toxicity." J Biol Chem **284**(30): 20329-20339.

Johnson, J. O., J. Mandrioli, M. Benatar, Y. Abramzon, V. M. Van Deerlin, J. Q. Trojanowski*, et al.* (2010). "Exome sequencing reveals VCP mutations as a cause of familial ALS." Neuron **68**(5): 857-864.

Josephs, K. A., M. E. Murray, J. L. Whitwell, N. Tosakulwong, S. D. Weigand, L. Petrucelli*, et al.* (2016). "Updated TDP-43 in Alzheimer's disease staging scheme." Acta Neuropathol **131**(4): 571-585.

Josephs, K. A., A. Stroh, B. Dugger and D. W. Dickson (2009). "Evaluation of subcortical pathology and clinical correlations in FTLD-U subtypes." Acta Neuropathol **118**(3): 349-358.

Jucker, M. and L. C. Walker (2011). "Pathogenic protein seeding in Alzheimer disease and other neurodegenerative disorders." Ann Neurol **70**(4): 532-540.

Kato, M., T. W. Han, S. Xie, K. Shi, X. Du, L. C. Wu*, et al.* (2012). "Cell-free formation of RNA granules: low complexity sequence domains form dynamic fibers within hydrogels." Cell **149**(4): 753-767.

Kawahara, Y. and A. Mieda-Sato (2012). "TDP-43 promotes microRNA biogenesis as a component of the Drosha and Dicer complexes." Proc Natl Acad Sci U S A **109**(9): 3347-3352.

Kovacs, G. G. (2016). "Molecular Pathological Classification of Neurodegenerative Diseases: Turning towards Precision Medicine." Int J Mol Sci **17**(2).

Kuiperij, H. B., A. A. Versleijen, M. Beenes, N. A. Verwey, L. Benussi, A. Paterlini*, et al.* (2017). "Tau Rather than TDP-43 Proteins are Potential Cerebrospinal Fluid Biomarkers for Frontotemporal Lobar Degeneration Subtypes: A Pilot Study." J Alzheimers Dis **55**(2): 585-595.

Kwong, L. K., K. Uryu, J. Q. Trojanowski and V. M. Lee (2008). "TDP-43 proteinopathies: neurodegenerative protein misfolding diseases without amyloidosis." Neurosignals **16**(1): 41-51.

Laferriere, F., Z. Maniecka, M. Perez-Berlanga, M. Hruska-Plochan, L. Gilhespy, E. M. Hock*, et al.* (2019). "TDP-43 extracted from frontotemporal lobar degeneration subject brains displays distinct aggregate assemblies and neurotoxic effects reflecting disease progression rates." Nat Neurosci **22**(1): 65-77.

Lagier-Tourenne, C., M. Polymenidou and D. W. Cleveland (2010). "TDP-43 and FUS/TLS: emerging roles in RNA processing and neurodegeneration." Hum Mol Genet **19**(R1): R46-64.

Lee, E. B., S. Porta, G. Michael Baer, Y. Xu, E. Suh, L. K. Kwong*, et al.* (2017). "Expansion of the classification of FTLD-TDP: distinct pathology associated with rapidly progressive frontotemporal degeneration." Acta Neuropathol **134**(1): 65-78.

Legname, G., I. V. Baskakov, H. O. Nguyen, D. Riesner, F. E. Cohen, S. J. DeArmond*, et al.* (2004). "Synthetic mammalian prions." Science **305**(5684): 673-676.

Lin, W. L. and D. W. Dickson (2008). "Ultrastructural localization of TDP-43 in filamentous neuronal inclusions in various neurodegenerative diseases." Acta Neuropathol **116**(2): 205-213.

Ling, S. C., M. Polymenidou and D. W. Cleveland (2013). "Converging mechanisms in ALS and FTD: disrupted RNA and protein homeostasis." Neuron **79**(3): 416-438.

Lukavsky, P. J., D. Daujotyte, J. R. Tollervey, J. Ule, C. Stuani, E. Buratti*, et al.* (2013). "Molecular basis of UG-rich RNA recognition by the human splicing factor TDP-43." Nat Struct Mol Biol **20**(12): 1443-1449.

Mackenzie, I. R., A. Baborie, S. Pickering-Brown, D. Du Plessis, E. Jaros, R. H. Perry*, et al.* (2006). "Heterogeneity of ubiquitin pathology in frontotemporal lobar degeneration: classification and relation to clinical phenotype." Acta Neuropathol **112**(5): 539-549.

Mackenzie, I. R., M. Neumann, A. Baborie, D. M. Sampathu, D. Du Plessis, E. Jaros*, et al.* (2011). "A harmonized classification system for FTLD-TDP pathology." Acta Neuropathol **122**(1): 111-113.

Mackenzie, I. R. and R. Rademakers (2008). "The role of transactive response DNA-binding protein-43 in amyotrophic lateral sclerosis and frontotemporal dementia." Curr Opin Neurol **21**(6): 693-700.

Maniecka, Z. and M. Polymenidou (2015). "From nucleation to widespread propagation: A prion-like concept for ALS." Virus Res **207**: 94-105.

Mann, J. R., A. M. Gleixner, J. C. Mauna, E. Gomes, M. R. DeChellis-Marks, P. G. Needham*, et al.* (2019). "RNA Binding Antagonizes Neurotoxic Phase Transitions of TDP-43." Neuron **102**(2): 321-338 e328.

Maruyama, H., H. Morino, H. Ito, Y. Izumi, H. Kato, Y. Watanabe*, et al.* (2010). "Mutations of optineurin in amyotrophic lateral sclerosis." Nature **465**(7295): 223-226.

Masrori, P. and P. Van Damme (2020). "Amyotrophic lateral sclerosis: a clinical review." Eur J Neurol.

McKhann, G. M., D. S. Knopman, H. Chertkow, B. T. Hyman, C. R. Jack, Jr., C. H. Kawas*, et al.* (2011). "The diagnosis of dementia due to Alzheimer's disease: recommendations from the National Institute on Aging-Alzheimer's Association workgroups on diagnostic guidelines for Alzheimer's disease." Alzheimers Dement **7**(3): 263-269.

Molliex, A., J. Temirov, J. Lee, M. Coughlin, A. P. Kanagaraj, H. J. Kim*, et al.* (2015). "Phase separation by low complexity domains promotes stress granule assembly and drives pathological fibrillization." Cell **163**(1): 123-133.

Mompean, M., M. Baralle, E. Buratti and D. V. Laurents (2016). "An Amyloid-Like Pathological Conformation of TDP-43 Is Stabilized by Hypercooperative Hydrogen Bonds." Front Mol Neurosci **9**: 125.

Moore, R. A., L. M. Taubner and S. A. Priola (2009). "Prion protein misfolding and disease." Curr Opin Struct Biol **19**(1): 14-22.

Morales, R., K. Abid and C. Soto (2007). "The prion strain phenomenon: molecular basis and unprecedented features." Biochim Biophys Acta **1772**(6): 681-691.

Morales, R., I. Moreno-Gonzalez and C. Soto (2013). "Cross-seeding of misfolded proteins: implications for etiology and pathogenesis of protein misfolding diseases." PLoS Pathog **9**(9): e1003537.

Murray, D. T., M. Kato, Y. Lin, K. R. Thurber, I. Hung, S. L. McKnight*, et al.* (2017). "Structure of FUS Protein Fibrils and Its Relevance to Self-Assembly and Phase Separation of Low-Complexity Domains." Cell **171**(3): 615-627 e616.

Nakashima-Yasuda, H., K. Uryu, J. Robinson, S. X. Xie, H. Hurtig, J. E. Duda*, et al.* (2007). "Co-morbidity of TDP-43 proteinopathy in Lewy body related diseases." Acta Neuropathol **114**(3): 221-229.

Neary, D., J. S. Snowden, L. Gustafson, U. Passant, D. Stuss, S. Black*, et al.* (1998). "Frontotemporal lobar degeneration: a consensus on clinical diagnostic criteria." Neurology **51**(6): 1546-1554.

Nehls, J., H. Koppensteiner, R. Brack-Werner, T. Floss and M. Schindler (2014). "HIV-1 replication in human immune cells is independent of TAR DNA binding protein 43 (TDP-43) expression." PLoS One **9**(8): e105478.

Neumann, M., L. K. Kwong, D. M. Sampathu, J. Q. Trojanowski and V. M. Lee (2007a). "TDP-43 proteinopathy in frontotemporal lobar degeneration and amyotrophic lateral sclerosis: protein misfolding diseases without amyloidosis." Arch Neurol **64**(10): 1388-1394.

Neumann, M., I. R. Mackenzie, N. J. Cairns, P. J. Boyer, W. R. Markesbery, C. D. Smith*, et al.* (2007b). "TDP-43 in the ubiquitin pathology of frontotemporal dementia with VCP gene mutations." J Neuropathol Exp Neurol **66**(2): 152-157.

Neumann, M., D. M. Sampathu, L. K. Kwong, A. C. Truax, M. C. Micsenyi, T. T. Chou*, et al.* (2006). "Ubiquitinated TDP-43 in frontotemporal lobar degeneration and amyotrophic lateral sclerosis." Science **314**(5796): 130-133.

Nishimura, A. L., M. Mitne-Neto, H. C. Silva, A. Richieri-Costa, S. Middleton, D. Cascio*, et al.* (2004). "A mutation in the vesicle-trafficking protein VAPB causes late-onset spinal muscular atrophy and amyotrophic lateral sclerosis." Am J Hum Genet **75**(5): 822-831.

Nonaka, T. and M. Hasegawa (2018). "TDP-43 Prions." Cold Spring Harb Perspect Med **8**(3).

Nonaka, T., M. Masuda-Suzukake, T. Arai, Y. Hasegawa, H. Akatsu, T. Obi*, et al.* (2013). "Prion-like properties of pathological TDP-43 aggregates from diseased brains." Cell Rep **4**(1): 124-134.

Noto, Y., K. Shibuya, Y. Sato, K. Kanai, S. Misawa, S. Sawai*, et al.* (2011). "Elevated CSF TDP-43 levels in amyotrophic lateral sclerosis: specificity, sensitivity, and a possible prognostic value." Amyotroph Lateral Scler **12**(2): 140-143.

Orru, C. D., M. Bongianni, G. Tonoli, S. Ferrari, A. G. Hughson, B. R. Groveman*, et al.* (2014). "A test for Creutzfeldt-Jakob disease using nasal brushings." N Engl J Med **371**(6): 519-529.

Orru, C. D., B. R. Groveman, A. G. Hughson, G. Zanusso, M. B. Coulthart and B. Caughey (2015). "Rapid and sensitive RT-QuIC detection of human Creutzfeldt-Jakob disease using cerebrospinal fluid." MBio **6**(1).

Ou, S. H., F. Wu, D. Harrich, L. F. Garcia-Martinez and R. B. Gaynor (1995). "Cloning and characterization of a novel cellular protein, TDP-43, that binds to human immunodeficiency virus type 1 TAR DNA sequence motifs." J Virol **69**(6): 3584-3596.

Parkinson, N., P. G. Ince, M. O. Smith, R. Highley, G. Skibinski, P. M. Andersen*, et al.* (2006). "ALS phenotypes with mutations in CHMP2B (charged multivesicular body protein 2B)." Neurology **67**(6): 1074-1077.

Peelaerts, W., L. Bousset, V. Baekelandt and R. Melki (2018). "a-Synuclein strains and seeding in Parkinson's disease, incidental Lewy body disease, dementia with Lewy bodies and multiple system atrophy: similarities and differences." Cell Tissue Res **373**(1): 195-212.

Polymenidou, M., C. Lagier-Tourenne, K. R. Hutt, C. F. Bennett, D. W. Cleveland and G. W. Yeo (2012). "Misregulated RNA processing in amyotrophic lateral sclerosis." Brain Res **1462**: 3-15.

Polymenidou, M., C. Lagier-Tourenne, K. R. Hutt, S. C. Huelga, J. Moran, T. Y. Liang*, et al.* (2011). "Long pre-mRNA depletion and RNA missplicing contribute to neuronal vulnerability from loss of TDP-43." Nat Neurosci **14**(4): 459-468.

Porta, S., Y. Xu, C. R. Restrepo, L. K. Kwong, B. Zhang, H. J. Brown*, et al.* (2018). "Patient-derived frontotemporal lobar degeneration brain extracts induce formation and spreading of TDP-43 pathology in vivo." Nat Commun **9**(1): 4220.

Prusiner, S. B. (1982). "Novel proteinaceous infectious particles cause scrapie." Science **216**(4542): 136-144.

Prusiner, S. B. (1998). "Prions." Proc Natl Acad Sci U S A **95**(23): 13363-13383.

Prusiner, S. B. (2013). "Biology and genetics of prions causing neurodegeneration." Annu Rev Genet **47**: 601-623.

Rascovsky, K., J. R. Hodges, D. Knopman, M. F. Mendez, J. H. Kramer, J. Neuhaus*, et al.* (2011). "Sensitivity of revised diagnostic criteria for the behavioural variant of frontotemporal dementia." Brain **134**(Pt 9): 2456-2477.

Rasmussen, J., J. Mahler, N. Beschorner, S. A. Kaeser, L. M. Hasler, F. Baumann*, et al.* (2017). "Amyloid polymorphisms constitute distinct clouds of conformational variants in different etiological subtypes of Alzheimer's disease." Proc Natl Acad Sci U S A **114**(49): 13018-13023.

Ratti, A. and E. Buratti (2016). "Physiological functions and pathobiology of TDP-43 and FUS/TLS proteins." J Neurochem **138 Suppl 1**: 95-111.

Renton, A. E., E. Majounie, A. Waite, J. Simon-Sanchez, S. Rollinson, J. R. Gibbs*, et al.* (2011). "A hexanucleotide repeat expansion in C9ORF72 is the cause of chromosome 9p21-linked ALS-FTD." Neuron **72**(2): 257-268.

Robinson, J. L., F. Geser, A. Stieber, M. Umoh, L. K. Kwong, V. M. Van Deerlin*, et al.* (2013). "TDP-43 skeins show properties of amyloid in a subset of ALS cases." Acta Neuropathol **125**(1): 121-131.

Saijo, E., B. Ghetti, G. Zanusso, A. Oblak, J. L. Furman, M. I. Diamond*, et al.* (2017). "Ultrasensitive and selective detection of 3-repeat tau seeding activity in Pick disease brain and cerebrospinal fluid." Acta Neuropathol **133**(5): 751-765.

Saini, A. and V. S. Chauhan (2011). "Delineation of the core aggregation sequences of TDP-43 C-terminal fragment." Chembiochem **12**(16): 2495-2501.

Salvadores, N., M. Shahnawaz, E. Scarpini, F. Tagliavini and C. Soto (2014). "Detection of misfolded Abeta oligomers for sensitive biochemical diagnosis of Alzheimer's disease." Cell Rep **7**(1): 261-268.

Sanders, D. W., S. K. Kaufman, S. L. DeVos, A. M. Sharma, H. Mirbaha, A. Li*, et al.* (2014). "Distinct tau prion strains propagate in cells and mice and define different tauopathies." Neuron **82**(6): 1271-1288.

Scialo, C., E. De Cecco, P. Manganotti and G. Legname (2019). "Prion and Prion-Like Protein Strains: Deciphering the Molecular Basis of Heterogeneity in Neurodegeneration." Viruses **11**(3).

Shahnawaz, M., A. Mukherjee, S. Pritzkow, N. Mendez, P. Rabadia, X. Liu*, et al.* (2020). "Discriminating alpha-synuclein strains in Parkinson's disease and multiple system atrophy." Nature **578**(7794): 273-277.

Shahnawaz, M., T. Tokuda, M. Waragai, N. Mendez, R. Ishii, C. Trenkwalder*, et al.* (2017). "Development of a Biochemical Diagnosis of Parkinson Disease by Detection of alpha-Synuclein Misfolded Aggregates in Cerebrospinal Fluid." JAMA Neurol **74**(2): 163-172.

Shimonaka, S., T. Nonaka, G. Suzuki, S. Hisanaga and M. Hasegawa (2016). "Templated Aggregation of TAR DNA-binding Protein of 43 kDa (TDP-43) by Seeding with TDP-43 Peptide Fibrils." J Biol Chem **291**(17): 8896-8907.

Sieben, A., T. Van Langenhove, S. Engelborghs, J. J. Martin, P. Boon, P. Cras*, et al.* (2012). "The genetics and neuropathology of frontotemporal lobar degeneration." Acta Neuropathol **124**(3): 353-372.

Smethurst, P., J. Newcombe, C. Troakes, R. Simone, Y. R. Chen, R. Patani*, et al.* (2016). "In vitro prion-like behaviour of TDP-43 in ALS." Neurobiol Dis **96**: 236-247.

Smethurst, P., K. C. Sidle and J. Hardy (2015). "Review: Prion-like mechanisms of transactive response DNA binding protein of 43 kDa (TDP-43) in amyotrophic lateral sclerosis (ALS)." Neuropathol Appl Neurobiol **41**(5): 578-597.

Steinacker, P., C. Hendrich, A. D. Sperfeld, S. Jesse, C. A. von Arnim, S. Lehnert*, et al.* (2008). "TDP-43 in cerebrospinal fluid of patients with frontotemporal lobar degeneration and amyotrophic lateral sclerosis." Arch Neurol **65**(11): 1481-1487.

Strong, M. J., G. M. Grace, M. Freedman, C. Lomen-Hoerth, S. Woolley, L. H. Goldstein*, et al.* (2009). "Consensus criteria for the diagnosis of frontotemporal cognitive and behavioural syndromes in amyotrophic lateral sclerosis." Amyotroph Lateral Scler **10**(3): 131-146.

Strong, M. J. and W. Yang (2011). "The frontotemporal syndromes of ALS. Clinicopathological correlates." J Mol Neurosci **45**(3): 648-655.

Suarez-Calvet, M., O. Dols-Icardo, A. Llado, R. Sanchez-Valle, I. Hernandez, G. Amer*, et al.* (2014). "Plasma phosphorylated TDP-43 levels are elevated in patients with frontotemporal dementia carrying a C9orf72 repeat expansion or a GRN mutation." J Neurol Neurosurg Psychiatry **85**(6): 684-691.

Teyssou, E., T. Takeda, V. Lebon, S. Boillee, B. Doukoure, G. Bataillon*, et al.* (2013). "Mutations in SQSTM1 encoding p62 in amyotrophic lateral sclerosis: genetics and neuropathology." Acta Neuropathol **125**(4): 511-522.

Thorpe, J. R., H. Tang, J. Atherton and N. J. Cairns (2008). "Fine structural analysis of the neuronal inclusions of frontotemporal lobar degeneration with TDP-43 proteinopathy." J Neural Transm (Vienna) **115**(12): 1661-1671.

Tollervey, J. R., T. Curk, B. Rogelj, M. Briese, M. Cereda, M. Kayikci*, et al.* (2011). "Characterizing the RNA targets and position-dependent splicing regulation by TDP-43." Nat Neurosci **14**(4): 452-458.

Uchino, A., M. Takao, H. Hatsuta, H. Sumikura, Y. Nakano, A. Nogami*, et al.* (2015). "Incidence and extent of TDP-43 accumulation in aging human brain." Acta Neuropathol Commun **3**: 35.

Uryu, K., H. Nakashima-Yasuda, M. S. Forman, L. K. Kwong, C. M. Clark, M. Grossman*, et al.* (2008). "Concomitant TAR-DNA-binding protein 43 pathology is present in Alzheimer disease and corticobasal degeneration but not in other tauopathies." J Neuropathol Exp Neurol **67**(6): 555-564.

Van Langenhove, T., J. van der Zee and C. Van Broeckhoven (2012). "The molecular basis of the frontotemporal lobar degeneration-amyotrophic lateral sclerosis spectrum." Ann Med **44**(8): 817-828.

van Rumund, A., A. J. E. Green, G. Fairfoul, R. A. J. Esselink, B. R. Bloem and M. M. Verbeek (2019). "alpha-Synuclein real-time quaking-induced conversion in the cerebrospinal fluid of uncertain cases of parkinsonism." Ann Neurol **85**(5): 777-781.

Walker, L. C. and M. Jucker (2015). "Neurodegenerative diseases: expanding the prion concept." Annu Rev Neurosci **38**: 87-103.

Warren, J. D., J. D. Rohrer and M. N. Rossor (2013). "Clinical review. Frontotemporal dementia." BMJ **347**: f4827.

Yokota, O., Y. Davidson, E. H. Bigio, H. Ishizu, S. Terada, T. Arai*, et al.* (2010). "Phosphorylated TDP-43 pathology and hippocampal sclerosis in progressive supranuclear palsy." Acta Neuropathol **120**(1): 55-66.

Zhang, P., B. Fan, P. Yang, J. Temirov, J. Messing, H. J. Kim*, et al.* (2019). "Chronic optogenetic induction of stress granules is cytotoxic and reveals the evolution of ALS-FTD pathology." Elife **8**.